Author(s): Kostensalo, Joel; Suhonen, Jouni

Title: Spin-multipole nuclear matrix elements in the pn quasiparticle random-phase approximation: Implications for β and ββ half-lives

Year: 2017

Version:

Please cite the original version:

Kostensalo, J., & Suhonen, J. (2017). Spin-multipole nuclear matrix elements in the pn quasiparticle random-phase approximation: Implications for β and ββ half-lives. Physical Review C, 95(1), Article 014322. https://doi.org/10.1103/PhysRevC.95.014322

Spin-multipole nuclear matrix elements in the *pn* quasiparticle random-phase approximation: Implications for β and $\beta\beta$ half-lives

Joel Kostensalo* and Jouni Suhonen†
University of Jyvaskyla, Department of Physics, P.O. Box 35, FI-40014 Jyvaskyla, Finland
(Received 17 August 2016; revised manuscript received 22 November 2016; published 20 January 2017)

Half-lives for 148 potentially measurable 2nd-, 3rd-, 4th-, 5th-, 6th-, and 7th-forbidden unique beta transitions are predicted. To achieve this, the ratio of the nuclear matrix elements (NMEs), calculated by the proton-neutron quasiparticle random-phase approximation (pnQRPA), M_{pnQRPA}, and a two-quasiparticle (two-qp) model, M_{qp}, is studied and compared with earlier calculations for the allowed Gamow-Teller (GT) 1^+ and first-forbidden spin-dipole (SD) 2^- transitions. The present calculations are done using realistic single-particle model spaces and G-matrix based microscopic two-body interactions. In terms of the ratio $k = M_{\mathrm{pnQRPA}}/M_{\mathrm{qp}}$ the studied decays fall into two groups: for GROUP 1, which consists of transitions involving non-magic nuclei, the ratio turns out to be $k = 0.29 \pm 0.15$. For GROUP 2, consisting of transitions involving semimagic nuclei, the ratio is 0.5–0.8 for half of the decays and less than 5×10^{-3} for the other half. The magnitudes of the NMEs for several nuclei of GROUP 2 depend sensitively on the size of the used single-particle space and the energies of few key single-particle orbitals used in the pnQRPA calculation, while no such dependence is found for the transitions involving nuclei of GROUP 1. Comparing the NME ratios k of GROUP 1 with those of the earlier GT and SD calculations, where also experimental data are available, the expected "experimental" half-lives for the decays between the 0^+ ground state of the even-even reference nuclei and the $J^\pi = 3^+,4^-,5^+,6^-,7^+,8^-$ states of the neighboring odd-odd nuclei are derived for possible experimental verification. The present results could also shed light to the magnitudes of the NMEs corresponding to the high-forbidden unique $0^+ \to J^\pi = 3^+,4^-,5^+,6^-,7^+,8^-$ virtual transitions taking part in the neutrinoless double beta decays.

DOI: 10.1103/PhysRevC.95.014322

I. INTRODUCTION

The (single) β-decay processes have been well understood for decades (see, e.g., [1]), and have been backed up by countless experiments. Recently, in the research of single β decay, transitions with ultralow Q values and of high forbiddenness have attracted attention [2–9]. However, predicting nuclear observables is not straightforward, and most nuclear models tend to produce good results only for some specific region(s) of the nuclear landscape. Recent research regarding the spin-dipole (SD) [10] and Gamow-Teller [11] nuclear matrix elements (NMEs) has shown that the observed NMEs of medium-heavy nuclei are reduced roughly by a constant factor compared to the ones predicted by the two-quasiparticle (two-qp) and proton-neutron random-phase approximation (pnQRPA) models. The reduction from the two-quasiparticle NME to that of the pnQRPA was denoted by k, and the reduction from the pnQRPA NME to the experimental NME was denoted by k_{NM}. We adopt the same notation in the present work. The reduction factor k was inferred to be caused by the spin-isospin correlations, whereas the reduction factor k_{NM} was interpreted to come from the nuclear medium and many-body effects not explicitly included in the two models. A similar study regarding the magnetic hexadecapole NMEs showed that the observed NME is reduced by a constant factor with respect to the NMEs of the two-qp model and the microscopic quasiparticle-phonon model (MQPM) [12].

In the present article we take a closer look at the suppression of the NMEs of the second- and higher-forbidden unique β decays when going from the two-qp level to the pnQRPA level of sophistication. The studied decays involve β^-, EC (electron capture), or β^+/EC (decaying by both the β^+ and EC channels) transitions. The transitions are overwhelmingly between ground states of medium-heavy nuclei and involve always an even-even reference nucleus and the adjacent odd-odd nucleus. To extend the scope of the present investigations we include also the known excited long-lived isomeric states of the odd-odd nuclei in our analysis. No experimental data exist for the half-lives of the discussed decays but some of them can, in principle, be measured to verify the predicted half-lives of the present work.

In a Kth forbidden ($K = 1,2,3,\ldots$) unique beta decay the difference in the angular momenta of the mother and daughter nuclei is $\Delta J = K + 1$, and the parity changes in the odd-forbidden and remains the same in the even-forbidden decays [13]. The change in angular momentum and parity for different degrees of forbiddenness is presented in Table I. Based on the suppression of the NMEs when going from the two-qp to the pnQRPA description, and on the earlier works on the suppression of the GT and SD NMEs, we make a prediction of the factor by which the true half-lives are increased with respect to the pnQRPA half-lives. The corresponding predicted half-lives can, in principle, be used to optimally design experiments for the measurement of the true half-lives of these transitions.

*joel.j.kostensalo@student.jyu.fi
†jouni.suhonen@phys.jyu.fi

TABLE I. The change in angular momentum and parity in a Kth forbidden unique β decay.

K	1	2	3	4	5	6	7
ΔJ	2	3	4	5	6	7	8
$\pi_i\pi_f$	-1	$+1$	-1	$+1$	-1	$+1$	-1

The nuclear β-decay research has recently been given a boost by the search for the double beta ($\beta\beta$) decays, in particular their neutrinoless variant ($0\nu\beta\beta$ decay), and by the astro-neutrino-nuclear processes involved in supernova detection. Studies of these processes aim at gaining knowledge on the nature of the neutrino, whether it is a Majorana particle or not, and absolute mass-scales of neutrinos [14–19]. The half-lives for $0\nu\beta\beta$ decays are extremely long, and competing processes, like the two-neutrino $\beta\beta$ ($2\nu\beta\beta$) decay, can make the detection of a $0\nu\beta\beta$ decay very hard. Sometimes highly forbidden beta decays compete with the $\beta\beta$ decay, like in the decay of ^{48}Ca where the experimentally observed $2\nu\beta\beta$ decay has competing nonunique and unique forbidden β decays to the 4^+, 5^+, and 6^+ states in ^{48}Ti [4,5]. What bridges the gap between the presently discussed highly-forbidden unique β decays and the $0\nu\beta\beta$ decay is the fact that the $0\nu\beta\beta$ decay is a two-step process where the 0^+ ground state of the initial even-even nucleus is connected to the virtual states of the intermediate odd-odd nucleus, which, in turn, are connected by similar transitions to the 0^+ ground state of the final even-even nucleus. Part of these connecting transitions are forbidden unique β transitions to and from the $J^\pi = 2^-,3^+,4^-,5^+,6^-,7^+,8^-$ intermediate states. This is why the suppression of the NMEs of high-forbidden unique β decays in the pnQRPA formalism is of great interest.

The theoretical prediction of β-decay and $\beta\beta$-decay half-lives is not without issues. The axial-vector coupling constant $g_{\rm A}$ and the particle-particle interaction parameter $g_{\rm pp}$ of pnQRPA have not been given an unambiguous value [20]. The $g_{\rm pp}$ values in the range 0.6–0.8 and quenched $g_{\rm A}$ values of approximately 0.6–0.7 seem to make the pnQRPA and experimental Gamow-Teller β and $2\nu\beta\beta$ NMEs agree [21,22]. The various issues concerning the determination of the value of $g_{\rm pp}$ are discussed in [23]. A more systematic determination of the $g_{\rm pp}$ values and effective values of $g_{\rm A}$ for Gamow-Teller ground-state to ground-state β decays is carried out in [24,25]. The decay rates depend on the second power of $g_{\rm A}$ for the β and on the fourth power for $\beta\beta$ decays, and so the understanding of the behavior of $g_{\rm A}$ is important for more accurate predictions of the half-lives. The mentioned studies have concentrated on examination of allowed and first-forbidden β decays but there are not many methods on the market which can study the quenching of $g_{\rm A}$ for higher-forbidden β transitions. One of these is the spectrum-shape method (SSM) introduced in [20]. In the SSM the shape of the energy spectrum of the emitted electrons in a (high-)forbidden nonunique beta decay is exploited to access the effective values of the weak coupling constants. The presently discussed forbidden unique β transitions can directly be used for the same purpose once experimental data for the corresponding half-lives become available.

II. THEORETICAL FORMALISM

In this section we give a short overview of the theory behind the performed calculations. The theoretical half-lives of Kth forbidden unique β decays are defined in terms of reduced transition probabilities $B_{K\rm u}$ and phase-space factors $f_{K\rm u}$. The $B_{K\rm u}$ is given by the NME, which in turn is given by the single-particle NMEs and one-body transition densities. The half-life can be written as (see [13] and Sec. II B below)

$$t_{1/2} = \frac{\kappa}{f_{K\rm u} B_{K\rm u}}, \tag{1}$$

where κ is a constant with value [26]

$$\kappa = \frac{2\pi^3\hbar^7 \ln 2}{m_e^5 c^4 (G_{\rm F}\cos\theta_{\rm C})^2} = 6147\ {\rm s}, \tag{2}$$

where $G_{\rm F}$ is the Fermi constant and $\theta_{\rm C}$ is the Cabibbo angle.

A. Phase-space factors

The phase-space factor $f_{K\rm u}^{(\pm)}$ for the Kth forbidden unique $\beta^\pm$ decay is [13]

$$f_{K\rm u}^{\mp} = \left(\frac{3}{4}\right)^K \frac{(2K)!!}{(2K+1)!!}\int_1^{E_0} S_{K\rm u}^{(\mp)}(Z_f,\epsilon)d\epsilon, \tag{3}$$

where $S_{K\rm u}^{(\mp)}$ is the shape function, which depends on the degree of forbiddenness. The shape function can be approximated, for example, using the *Primakoff-Rosen* approximation presented in Ref. [27], but, in order to get more realistic values for the phase-space factors, the exact expressions, presented in [28], are used in this work. The phase-space factor used for the EC decays is presented in [29]. The general formulation for calculating phase-space factors is presented rigorously in [1]. The nonunique case is also presented in detail in [3].

B. Reduced beta transition probability

The reduced beta transition probability can be written in terms of the NME $M_{K\rm u}$ as

$$B_{K\rm u} = \frac{g_{\rm A}^2}{2J_i+1}|M_{K\rm u}|^2, \tag{4}$$

where J_i is the angular momentum of the mother nucleus. For $g_{\rm A}$ we adopt here the value $g_{\rm A} = 1.25$ and calculate the β-decay half-lives by introducing the quenching into the computed NMEs. The NME in (4) can be expressed as [13]

$$M_{K\rm u} = \sum_{ab} M^{(K\rm u)}(ab)(\psi_f||[c_a^\dagger \tilde{c}_b]_{K+1}||\psi_i), \tag{5}$$

where the factors $M^{(K\rm u)}(ab)$ are the single-particle matrix elements and the quantities $(\psi_f||[c_a^\dagger\tilde{c}_b]_{K+1}||\psi_i)$ are the one-body transition densities, with ψ_i being the initial-state and ψ_f being the final-state nuclear wave functions. The operator $c_a^\dagger$ creates a nucleon and the operator $\tilde{c}_a$ annihilates a nucleon on orbital a (for more details see [13]). The single-particle matrix elements are given by [30]

$$M^{(K\rm u)}(ab) = (2.590\times 10^{-3}\times b\ [{\rm fm}])^K m^{(K\rm u)}(ab), \tag{6}$$

where b is the oscillator length given by

$$b = \frac{197.33}{\sqrt{940 \times (45A^{1/3} - 25A^{-2/3})}}\ \text{fm}. \quad (7)$$

In Eq. (6) the quantity $m^{(K\mathrm{u})}(ab)$ is the scaled single-particle matrix element given in the Biedenharn-Rose (BR) phase convention as

$$\begin{aligned} m^{(K\mathrm{u})}(ab) = {} & (-1)^{(l_b - l_a + K)/2} \times \frac{1}{2\sqrt{(K+1)(2K+3)}} \\ & \times (-1)^{l_a + j_a + j_b + K + 1} \times \frac{1 + (-1)^{l_a + l_b + K}}{2} \hat{j}_a \hat{j}_b \\ & \times \begin{pmatrix} j_a & j_b & K+1 \\ \frac{1}{2} & \frac{-1}{2} & 0 \end{pmatrix} \\ & \times \left[(-1)^K \hat{j}_a^{\,2} + (-1)^{j_a + j_b + 1} \hat{j}_b^{\,2} \right. \quad (8) \\ & \left. + 2(K+1)(-1)^{l_a + j_a + K - \frac{1}{2}} \right] \tilde{R}^{(K)}_{ab}, \quad (9) \end{aligned}$$

where the j_i and l_i stand for the total angular momentum and orbital angular momentum of the orbital i, respectively, and $\tilde{R}^{(K)}_{ab}$ is the scaled radial integral. The calculation of the values of the radial integrals is discussed in detail in [13]. The BR phase convention is used in the calculations, since then in the BCS picture all vacancy amplitudes are positive, whereas in the Condon-Shortley (CS) convention the sign depends on l_i.

The one-body transition densities in (5) can be written in the pnQRPA picture for β^- decays as [31]

$$(\omega_f || [c_p^\dagger \tilde{c}_n]_K || 0^+_{\text{g.s.}}) = \delta_{K J_f} \hat{J}_f \left(u_p v_n X^{\omega_f}_{pn} + v_p u_n Y^{\omega_f}_{pn} \right) \quad (10)$$

and for β^+/EC decays as

$$(\omega_f || [c_n^\dagger \tilde{c}_p]_K || 0^+_{\text{g.s.}}) = \delta_{K J_f} \hat{J}_f \left(u_n v_p X^{\omega_f}_{pn} + v_n u_p Y^{\omega_f}_{pn} \right), \quad (11)$$

where the pnQRPA vacuum is the 0^+ ground state of the even-even reference nucleus of the transition, and u and v are the vacancy and occupation amplitudes given by the BCS calculation [13]. The two-qp matrix element can be obtained from (10) and (11) by setting $X = 1$ and $Y = 0$. The final state ω_f can be written as [32]

$$|\omega_f\rangle = \sum_{pn} \left(X^{\omega_f}_{pn} [a_p^\dagger a_n^\dagger]_{J_f} + Y^{\omega_f}_{pn} [\tilde{a}_p \tilde{a}_n]_{J_f} \right) |\text{pnQRPA}\rangle, \quad (12)$$

where X and Y are the forward- and backward-going amplitudes, $a^\dagger$ and $\tilde{a}$ are the BCS quasiparticle creation and annihilation operators, and $|\text{pnQRPA}\rangle$ is the pnQRPA vacuum.

The proton and neutron pairing gaps Δ_p and Δ_n needed for solving the BCS equations can be calculated using the three-point formulas [33,34]

$$\begin{aligned} \Delta_p(A,Z) = {} & \tfrac{1}{4}(-1)^{Z+1} [S_p(A+1,Z+1) \\ & - 2S_p(A,Z) + S_p(A-1,Z-1)], \\ \Delta_n(A,Z) = {} & \tfrac{1}{4}(-1)^{A-Z+1} [S_n(A+1,Z) \\ & - 2S_n(A,Z) + S_n(A-1,Z)], \end{aligned} \quad (13)$$

where S_p is the proton separation energy and S_n the neutron separation energy.

III. NUMERICAL APPLICATION OF THE FORMALISM

Half-lives and partial half-lives were calculated for 148 β^-, EC, and β^+/EC transitions. This was done with both the two-qp model and the more advanced pnQRPA approach. In the two-qp model the transition is presumed to happen between the two single-particle states which give the largest absolute value for the two-qp NME, while, in the pnQRPA configuration, mixing of all possible proton-neutron configurations, producing the state of interest in the involved odd-odd nucleus, is taken into consideration.

The single-particle energies needed to solve the BCS equations were calculated using the Woods-Saxon potential with the Bohr-Mottelson parametrization [35] in a small model space with an inert core. For nuclei with mass number $A = 50$–60 the core was chosen to consist of eight protons and neutrons with the valence space spanning the range $0d_{5/2}$–$0g_{9/2}$. For the nuclei with larger A a core of 20 protons and neutrons was assumed. For $A = 74$ the valence space was spanned by the single-particle orbitals in the range $0f_{7/2}$–$0h_{11/2}$, for $A = 84$–108 in the range $0f_{7/2}$–$0h_{9/2}$, and for $A = 110$–146 in the range $0f_{7/2}$–$2p_{1/2}$. For each degree of forbiddenness one NME associated with an electron capture and a β^- transition was calculated in the so-called large no-core model space, where an inert core was not assumed and additional, higher lying, (quasistationary) single-particle states were added. This was done to test if the expanding of the model space had any effect on the calculated half-lives. For the third-forbidden decays only the electron-capture case was studied, since there were no third-forbidden β^- decays in the studied transitions. The proton and neutron Fermi surfaces were well contained in the used model spaces to guarantee a realistic BCS treatment of the quasiparticle correlations. The residual interaction used for both the BCS and the pnQRPA was the Bonn-A G matrix [36]. The particle-hole and particle-particle two-body interaction matrix elements were scaled by the corresponding parameters g_{ph} and g_{pp} (see, e.g. [32]). For the present calculations the default values $g_{\text{ph}} = 1.0$ and $g_{\text{pp}} = 1.0$ were adopted. The uncertainties of the computed half-lives due to the errors in the NMEs were approximated by letting these two parameters vary by 10% from the default value. The dependence of the nuclear matrix elements on the parameters g_{pp} and g_{ph} was examined by calculating the values of a selected set of decays in both the large and the small model space for different values of the two parameters.

The computed pairing gaps were adjusted to fit the experimental values by tuning the pairing parameters g^p_{pair} and g^n_{pair}. The experimental values were calculated using the three-point formulas (13) and the experimental separation energies given in [37]. The values used for the pairing parameters are listed in Tables II and III.

The Q values and their experimental errors, found in [38], were used for the calculation of the phase-space factors [28] and their uncertainties. The value of the nuclear-medium/many-body reduction factor k_{NM} was inferred from [11]. We use an uncertainty of 10% for this factor. The contribution of these uncertainties, along with the uncertainties arising from the computed NMEs, was taken into account in the error estimation of the computed half-lives.

TABLE II. Renormalization parameters of pairing interaction for the studied even-even reference nuclei in the mass region $A = 50$–102. In the second column the parameter $g^n_{\rm pair}$ for neutrons is given, and in the third column the parameter $g^p_{\rm pair}$ for protons is given.

Nucleus	$g^n_{\rm pair}$	$g^p_{\rm pair}$
^{50}Ca	1.185	0.923
^{50}Cr	1.09	1.165
^{50}Ti	1.12	1.126
^{52}Cr	1.08	0.945
^{52}Ti	1.19	1.125
^{54}Cr	1.19	1.16
^{54}Fe	1.06	1.07
^{54}Ni	1.162	0.88
^{56}Cr	1.19	1.14
^{56}Fe	1.18	1.08
^{58}Fe	0.98	1.15
^{58}Ni	1.075	0.953
^{60}Fe	0.955	1.115
^{60}Ni	0.98	1.07
^{62}Fe	1.025	1.06
^{62}Ni	1.04	0.953
^{74}Kr	1.16	0.972
^{74}Se	1.14	1.05
^{84}Kr	1.083	0.91
^{84}Se	1.00	0.976
^{84}Sr	1.10	0.92
^{86}Kr	0.975	0.937
^{86}Sr	1.155	1.02
^{86}Zr	1.26	1.07
^{88}Mo	1.21	1.12
^{88}Sr	0.95	0.95
^{88}Zr	1.152	0.96
^{90}Kr	1.105	0.938
^{90}Mo	1.159	1.072
^{90}Sr	1.162	0.961
^{90}Zr	0.912	0.87
^{92}Mo	0.885	1.01
^{92}Zr	1.17	0.92
^{94}Mo	1.165	1.06
^{94}Ru	0.88	1.025
^{94}Zr	0.93	0.88
^{96}Mo	1.02	1.062
^{96}Pd	1.115	1.02
^{96}Ru	1.154	1.105
^{98}Mo	0.95	1.11
^{98}Pd	1.13	1.057
^{98}Ru	1.09	1.185
^{98}Zr	0.76	1.01
^{100}Cd	1.115	1.02
^{100}Mo	0.98	0.99
^{100}Pd	1.12	1.088
^{100}Ru	1.03	1.19
^{100}Zr	0.91	0.90
^{102}Cd	1.11	1.055
^{102}Pd	1.05	1.105

TABLE III. Same as table II for mass region $A = 104$–146.

Nucleus	$g^n_{\rm pair}$	$g^p_{\rm pair}$
^{104}Cd	1.05	1.08
^{104}Mo	0.90	0.98
^{104}Pd	0.988	1.12
^{104}Ru	1.02	0.976
^{106}Cd	1.00	1.005
^{106}Sn	1.15	0.60
^{108}Cd	1.00	1.10
^{108}Sn	0.985	0.705
^{110}Cd	0.97	1.10
^{110}Sn	1.015	0.88
^{110}Te	1.02	0.928
^{112}Sn	0.98	0.79
^{112}Te	1.01	0.995
^{114}Cd	0.985	1.077
^{114}Sn	0.968	0.74
^{114}Te	0.955	0.995
^{116}Cd	1.003	1.073
^{116}Sn	0.905	0.67
^{116}Te	1.05	0.93
^{118}Cd	0.885	0.947
^{118}Sn	0.91	0.50
^{120}Cd	0.95	0.946
^{120}Pd	0.98	0.946
^{120}Sn	0.89	0.56
^{120}Te	0.90	0.93
^{122}Cd	0.983	0.935
^{122}Sn	0.94	0.52
^{122}Te	0.89	0.93
^{124}Cd	1.00	0.93
^{124}Sn	0.98	0.40
^{124}Te	1.139	0.942
^{126}Sn	1.095	0.60
^{126}Te	1.09	0.915
^{128}Sn	1.115	0.68
^{128}Te	1.100	0.89
^{130}Ba	1.09	0.985
^{130}Ce	1.05	0.955
^{130}Sn	1.065	0.67
^{130}Te	1.079	0.88
^{130}Xe	1.079	0.965
^{132}Ba	0.967	1.00
^{132}Ce	1.164	1.06
^{132}Sn	0.90	0.75
^{132}Te	1.025	0.88
^{134}Ba	1.065	0.965
^{134}Ce	1.085	0.985
^{134}Nd	1.066	1.076
^{134}Te	1.205	0.90
^{134}Xe	1.065	0.89
^{136}Ba	1.025	0.935
^{136}Te	1.25	0.697
^{136}Xe	0.90	0.842
^{138}Ba	1.19	0.875
^{138}Ce	1.04	0.97
^{138}Xe	1.25	0.92
^{146}Gd	0.90	0.90
^{146}Sm	1.24	0.935

IV. RESULTS AND DISCUSSION

The main results of this article are presented in Tables IV–X, and below we discuss how they were obtained.

A. Nuclear matrix elements and half-lives for the two-quasiparticle and pnQRPA models

The pnQRPA and two-qp-model calculated NMEs (columns 4 and 5) and the corresponding phase-space factors and expected half-lives, including their uncertainties (columns 6 and 7), are listed in Tables IV–X for each degree of forbiddenness separately. In column 1 the corresponding transition and in column 2 the decay mode are given. Column 3 lists the proton-neutron configuration responsible for the two-qp NME. Most of the studied decay transitions are ground-state to ground-state, but to widen the scope of the present study, transitions between a ground state and an excited state were studied in cases where the excited state was measured to be isomeric, i.e. having an exceptionally long γ-decay half-life. The isomeric states involved in the calculations are marked by an asterisk in Tables IV–X.

The β-decay half-lives vary by many orders of magnitude mainly because of the varying degree of forbiddenness. As a rule of thumb, a decrease or increase of the Q value of about 1 MeV, or whether the decay is to or from the pnQRPA vacuum, both increase or decrease the half-life by approximately one order of magnitude. On the other hand, one degree of forbiddenness changes the half-life by close to four orders of magnitude. For example, in the case of the second-forbidden decays, the variation in the Q value alone, from around 1 MeV [^{54}Mn(3^+) $\rightarrow$ ^{54}Fe(0^+)] to the enormous 9.3 MeV [^{52}Sc(3^+) $\rightarrow$ ^{52}Ti(0^+)] is enough to make a difference of up to nine orders of magnitude in the half-lives. This is purely a phase-space effect and has no exotic origin like interfering atomic effects (unlike in the case of the ultra-low Q values, see Refs. [6–9]), due to the fact that even the smaller Q value is of the order of 1 MeV, well suitable for the phase-space description of the present work.

Many of the studied decays are part of a long decay chain, including decays with different degrees of forbiddenness. In Fig. 1 a simple decay chain, including some of the studied $A = 110$ nuclei, is presented. The chain consists purely of ground-state to ground-state β^+ and β^+/EC decays. In Fig. 2 a more complicated $A = 96$ chain is presented. This chain includes both β^+/EC and β^- decays, and some of the decays are to or from a first excited state which is a long-lived isomer.

In order to determine how the experimental values of the half-lives of these decays will most likely differ from the values given by the models, we compare our results to the earlier results for the Gamow-Teller (GT) 1^+ and the first-forbidden spin-dipole (SD) 2^- decays. In the latter case [10] the authors compared the values of the experimental, pnQRPA-calculated and two-qp-calculated SD NMEs. It was found that the ratio $k = M_{\mathrm{QRPA}}/M_{\mathrm{qp}}$ was approximately 0.4, while the ratio $k_{\mathrm{NM}} = M_{\mathrm{exp}}/M_{\mathrm{QRPA}}$ was about 0.5. In this study the geometric mean of the β^+ and β^- NMEs, with a common mother or daughter nucleus, was used in the evaluation of the ratios. The geometric mean of n real numbers $a_1, \ldots, a_n$ is defined as

$$m_{\mathrm{geom}} = \left(\prod_{i=1}^{n} a_i\right)^{1/n}, \tag{14}$$

and in the case of the studied SD matrix elements it reduces to

$$m_{\mathrm{geom}} = [M^-(\mathrm{SD2})M^+(\mathrm{SD2})]^{1/2}, \tag{15}$$

where $M^{\pm}$(SD2) is the transition matrix element for the $\beta^{\pm}$ transition $2^- \rightarrow 0^+$ [10]. In the study [11], regarding the mean matrix elements of the GT decays, the ratio k was found to be approximately 0.38, and the ratio k_{NM} was found to be about 0.6. This study included a large number of decays, and the behavior of k and k_{NM} as a function of A was determined in much more detail than in the earlier study regarding the SD NMEs. For the second- or higher-forbidden decays we do not have experimental data, but we can still calculate the ratio of the pnQRPA and two-qp NMEs. In case this ratio is close to the ones of GT and SD matrix elements, we can make a prediction of the ratio $k_{\mathrm{NM}} = M_{\mathrm{exp}}/M_{\mathrm{QRPA}}$ for the higher-forbidden decays by extrapolating from the k_{NM} of the GT and SD decays (see Sec. IV B).

The pairing gaps were adjusted to fit the experimental values of the pairing gaps by tuning the pairing parameters g^p_{pair} and g^n_{pair}. The pairing parameters used for the calculations of the nuclear matrix elements are listed in the Tables II and III.

In Tables IV–X it is seen that for most decays the NMEs given by pnQRPA are about 2–3 times smaller than those given by the two-qp model, regardless of the degree of forbiddenness. However, there seem to be some noticeable exceptions. The pnQRPA NMEs seem to be around 3–4 orders of magnitude smaller than those of the two-qp model for many of the decays including a semimagic even-even reference nucleus. Since the ratios of the corresponding NMEs are so different, it is best to study the ratio k separately for the (semi)magic and nonmagic reference nuclei. In Fig. 3 the ratios $M_{\mathrm{pnQRPA}}/M_{\mathrm{qp}}$ are given for decays including a nonmagic reference nucleus and in Fig. 4 for decays including a (semi)magic one. The degree of forbiddenness is given by the shape and color coding. For mass numbers with several NMEs calculated for the nonmagic cases, the geometric mean, defined in Eq. (14), was used as the value of k. For the (semi)magic cases the geometric mean was not used, since for some mass numbers A there were NMEs which could differ by three orders of magnitude, rendering the use of the geometric mean dubious. Unlike in the first-forbidden case, studied in [10], the variance of the geometric mean of decays with a common mother or daughter nucleus (see Fig. 5) did not seem to be significantly different than the variance of k for all decay transitions (see Fig. 3). Therefore, in the nonmagic case, the value of k was extracted from all calculated decays using the geometric mean (14) for the full isobaric chains.

In order to make the rest of the paper easier to follow let us label the decays with a nonmagic even-even reference nucleus GROUP 1 and the rest belong to GROUP 2. Exactly one half of the presently discussed transitions belong to GROUP 1, the other half to GROUP 2. The k values for GROUP 1 are presented in Fig. 3 and for GROUP 2 in Fig. 4. For GROUP 1

TABLE IV. Nuclear matrix elements and phase-space factors f for the second-forbidden unique β^-, β^+, and β^+/EC decays, computed by the pnQRPA and two-qp models. The corresponding two-qp p-n configuration is also given. The transitions are $0^+ \leftrightarrow 3^+$, where 0^+ is the ground state of the participating even-even nucleus. The involved excited isomeric states are marked with an asterisk (*). The expected "experimental" half-lives are scaled from the pnQRPA half-lives using the scaling factor ξ presented in Table XII.

Transition	Mode	p-n conf.	$\lvert M_{\mathrm{pnQRPA}}\rvert$ (fm^2)	$\lvert M_{\mathrm{qp}}\rvert$ (fm^2)	f	Expected $t_{1/2}$
^{52}V $\rightarrow$ ^{52}Cr	β^-	$0f_{7/2}$ - $1p_{1/2}$	4.94(4) $\times$ 10^{-6}	4.95 $\times$ 10^{-4}	1.66(4) $\times$ 10^{4}	4.7(9) $\times$ 10^{3} yr
^{52}Ti $\rightarrow$ ^{52}V	β^-	$0g_{9/2}$ - $0d_{3/2}$	2.42(2) $\times$ 10^{-4}	6.81 $\times$ 10^{-4}	66(2)	70(20) yr
^{52}Sc $\rightarrow$ ^{52}Ti	β^-	$0d_{3/2}$ - $0g_{9/2}$	1.98(2) $\times$ 10^{-4}	6.56 $\times$ 10^{-4}	1.98(3) $\times$ 10^{7}	22(5) h
^{54}V $\rightarrow$ ^{54}Cr	β^-	$0d_{3/2}$ - $0g_{9/2}$	2.52(2) $\times$ 10^{-4}	6.65 $\times$ 10^{-4}	1.92(4) $\times$ 10^{6}	6(2) d
^{54}Mn $\rightarrow$ ^{54}Fe	β^-	$0d_{3/2}$ - $0g_{9/2}$	3.52(2) $\times$ 10^{-4}	6.80 $\times$ 10^{-4}	3.86(5) $\times$ 10^{-2}	4.0(9) $\times$ 10^{5} yr
^{54}Mn $\rightarrow$ ^{54}Cr	EC	$0g_{9/2}$ - $0d_{3/2}$	1.88(2) $\times$ 10^{-4}	6.87 $\times$ 10^{-4}	8.70(18) $\times$ 10^{-2}	6(2) $\times$ 10^{5} yr
	β^+				7.29(11) $\times$ 10^{-5}	7(2) $\times$ 10^{8} yr
	EC/β^+				8.71(11) $\times$ 10^{-2}	6(2) $\times$ 10^{5} yr
^{56}Cr $\rightarrow$ ^{56}Mn	β^-	$0g_{9/2}$ - $0d_{3/2}$	2.47(2) $\times$ 10^{-4}	6.95 $\times$ 10^{-4}	16(2)	280(60) yr
^{56}Mn $\rightarrow$ ^{56}Fe	β^-	$0d_{3/2}$ - $0g_{9/2}$	2.78(2) $\times$ 10^{-4}	6.83 $\times$ 10^{-4}	1.01(5) $\times$ 10^{4}	2.5(6) yr
^{94}Nb* $\rightarrow$ ^{94}Mo	β^-	$0f_{5/2}$ - $0h_{11/2}$	3.12(2) $\times$ 10^{-4}	1.12 $\times$ 10^{-3}	186(12)	110(30) yr
^{94}Nb* $\rightarrow$ ^{94}Zr	EC	$0h_{11/2}$ - $0f_{5/2}$	3.85(3) $\times$ 10^{-4}	1.18 $\times$ 10^{-3}	3.38(5) $\times$ 10^{-2}	2.9(6) $\times$ 10^{5} yr
^{96}Pd $\rightarrow$ ^{96}Rh*	EC	$0h_{11/2}$ - $0f_{5/2}$	8.89(35) $\times$ 10^{-7}	1.19 $\times$ 10^{-3}	183(4)	1.9(4) $\times$ 10^{6} yr
	β^+				69.0(3)	5(1) $\times$ 10^{6} yr
	EC/β^+				252(7)	1.4(3) $\times$ 10^{6} yr
^{96}Rh* $\rightarrow$ ^{96}Ru	EC	$0h_{11/2}$ - $0f_{5/2}$	1.76(1) $\times$ 10^{-4}	1.18 $\times$ 10^{-3}	7.29(7) $\times$ 10^{3}	9(2) yr
	β^+				5.02(8) $\times$ 10^{4}	1.2(3) yr
	EC/β^+				5.75(9) $\times$ 10^{4}	1.1(3) yr
^{104}Mo $\rightarrow$ ^{104}Tc	β^-	$0f_{5/2}$ - $0h_{11/2}$	3.01(2) $\times$ 10^{-4}	1.14 $\times$ 10^{-3}	245(50)	26(6) yr
^{104}Tc $\rightarrow$ ^{104}Ru	β^-	$0f_{5/2}$ - $0h_{11/2}$	2.30(2) $\times$ 10^{-4}	1.11 $\times$ 10^{-3}	5.17(20) $\times$ 10^{5}	50(10) d
^{110}Te $\rightarrow$ ^{110}Sb	EC	$0f_{5/2}$ - $0h_{11/2}$	1.09(1) $\times$ 10^{-4}	1.21 $\times$ 10^{-3}	4.99(5) $\times$ 10^{3}	10(2) yr
	β^+				9.55(16) $\times$ 10^{3}	5(1) yr
	EC/β^+				1.45(3) $\times$ 10^{4}	3.4(7) yr
^{110}Sb $\rightarrow$ ^{110}Sn	EC	$0h_{11/2}$ - $0f_{5/2}$	1.46(1) $\times$ 10^{-4}	1.18 $\times$ 10^{-3}	5.78(7) $\times$ 10^{4}	3.3(7) yr
	β^+				6.1(2) $\times$ 10^{5}	120(30) d
	EC/β^+				6.7(2) $\times$ 10^{5}	110(30) d
^{112}Te $\rightarrow$ ^{112}Sb	EC	$0f_{5/2}$ - $0h_{11/2}$	2.95(2) $\times$ 10^{-4}	1.17 $\times$ 10^{-3}	744(23)	9(2) yr
	β^+				353(20)	19(4) yr
	EC/β^+				1.10(5) $\times$ 10^{3}	6(2) yr
^{112}Sb $\rightarrow$ ^{112}Sn	EC	$0h_{11/2}$ - $0f_{5/2}$	1.40(6) $\times$ 10^{-6}	1.24 $\times$ 10^{-3}	2.03(4) $\times$ 10^{4}	1.0(2) $\times$ 10^{5} yr
	β^+				1.13(3) $\times$ 10^{5}	1.9(5) $\times$ 10^{4} yr
	EC/β^+				1.33(4) $\times$ 10^{5}	1.6(4) $\times$ 10^{4} yr
^{114}Te $\rightarrow$ ^{114}Sb	EC	$0f_{5/2}$ - $0h_{11/2}$	2.10(2) $\times$ 10^{-4}	1.21 $\times$ 10^{-3}	53.1(5)	250(50) yr
	β^+				2.19(5)	6(2) $\times$ 10^{3} yr
	EC/β^+				55.3(6)	240(50) yr
^{114}Sb $\rightarrow$ ^{114}Sn	EC	$0h_{11/2}$ - $0f_{5/2}$	4.28(3) $\times$ 10^{-4}	1.25 $\times$ 10^{-3}	8.1(2) $\times$ 10^{3}	2.8(6) yr
	β^+				2.5(1) $\times$ 10^{4}	320(90) d
	EC/β^+				3.3(2) $\times$ 10^{4}	250(60) d
^{116}Te $\rightarrow$ ^{116}Sb	EC	$0f_{5/2}$ - $0h_{11/2}$	5.88(4) $\times$ 10^{-4}	1.16 $\times$ 10^{-3}	2.19(3)	800(200) yr
	β^+				5.9(3) $\times$ 10^{-4}	2.9(6) $\times$ 10^{7} yr
	EC/β^+				2.19(3)	800(200) yr
^{116}Sb $\rightarrow$ ^{116}Sn	EC	$0h_{11/2}$ - $0f_{5/2}$	5.29(4) $\times$ 10^{-4}	1.26 $\times$ 10^{-3}	1.75(2) $\times$ 10^{3}	8(2) yr
	β^+				1.85(3) $\times$ 10^{3}	8(2) yr
	EC/β^+				3.61(4) $\times$ 10^{3}	4(1) yr
^{120}Pd $\rightarrow$ ^{120}Ag	β^-	$0h_{11/2}$ - $0f_{5/2}$	4.52(3) $\times$ 10^{-4}	1.26 $\times$ 10^{-3}	4.10(4) $\times$ 10^{5}	5.6(6) d
^{120}Ag $\rightarrow$ ^{120}Cd	β^-	$0f_{5/2}$ - $0h_{11/2}$	3.30(3) $\times$ 10^{-4}	1.02 $\times$ 10^{-3}	1.61(1) $\times$ 10^{7}	2.9(8) d
^{130}Ce $\rightarrow$ ^{130}La	EC	$0h_{11/2}$ - $0f_{5/2}$	2.04(2) $\times$ 10^{-4}	9.89 $\times$ 10^{-4}	28.6(4)	500(100) yr
	β^+				2.00(6) $\times$ 10^{-1}	7(2) $\times$ 10^{4} yr
	EC/β^+				28.8(4)	500(100) yr
^{130}La $\rightarrow$ ^{130}Ba	EC	$0h_{11/2}$ - $0f_{5/2}$	5.40(4) $\times$ 10^{-4}	1.25 $\times$ 10^{-3}	8.09(3) $\times$ 10^{3}	1.7(4) yr
	β^+				1.09(6) $\times$ 10^{4}	1.3(3) yr
	EC/β^+				1.90(9) $\times$ 10^{4}	270(60) d
^{132}Sn $\rightarrow$ ^{132}Sb*	β^-	$0p_{1/2}$ - $1f_{7/2}$	7.98(28) $\times$ 10^{-11}	6.91 $\times$ 10^{-4}	5.45(6) $\times$ 10^{3}	1.7(4) $\times$ 10^{13} yr

TABLE V. The same as Table IV for the third-forbidden unique $0^+ \leftrightarrow 4^-$ transitions.

Transition	Mode	p-n conf.	$\lvert M_{\mathrm{pnQRPA}}\rvert$ (fm^3)	$\lvert M_{\mathrm{qp}}\rvert$ (fm^3)	f	Expected $t_{1/2}$
^{74}Kr $\rightarrow$ ^{74}Br*	EC	$1p_{3/2}$ - $1d_{5/2}$	7.29(5) $\times$ 10^{-6}	1.32 $\times$ 10^{-5}	11.3(3)	5(1) $\times$ 10^{5} yr
	β^+				1.12(4)	5(1) $\times$ 10^{6} yr
	EC/β^+				12.5(3)	4.1(9) $\times$ 10^{5} yr
^{74}Br* $\rightarrow$ ^{74}Se	EC	$1d_{5/2}$ - $1p_{3/2}$	4.96(4) $\times$ 10^{-6}	1.43 $\times$ 10^{-5}	2.13(2) $\times$ 10^{4}	500(200) yr
	β^+				3.04(4) $\times$ 10^{5}	330(80) yr
	EC/β^+				3.26(4) $\times$ 10^{5}	310(60) yr
^{86}Zr $\rightarrow$ ^{86}Y	EC	$1p_{3/2}$ - $1d_{5/2}$	5.89(4) $\times$ 10^{-6}	1.46 $\times$ 10^{-5}	4.1(5) $\times$ 10^{-2}	1.9(6) $\times$ 10^{8} yr
	β^+				1.9(6) $\times$ 10^{-7}	4(2) $\times$ 10^{13} yr
	EC/β^+				4.1(5) $\times$ 10^{-2}	1.9(6) $\times$ 10^{8} yr
^{86}Y $\rightarrow$ ^{86}Sr	EC	$1d_{5/2}$ - $1p_{3/2}$	9.21(6) $\times$ 10^{-6}	1.55 $\times$ 10^{-5}	2.64(6) $\times$ 10^{3}	1.1(3) $\times$ 10^{4} yr
	β^+				6.5(3) $\times$ 10^{3}	4(2) $\times$ 10^{3} yr
	EC/β^+				9.2(3) $\times$ 10^{3}	3.2(7) $\times$ 10^{3} yr
^{88}Mo $\rightarrow$ ^{88}Nb	EC	$1p_{3/2}$ - $1d_{5/2}$	6.61(5) $\times$ 10^{-6}	1.49 $\times$ 10^{-5}	131(2)	5(1) $\times$ 10^{4} yr
	β^+				30.2(8)	2.1(5) $\times$ 10^{5} yr
	EC/β^+				162(3)	3.9(8) $\times$ 10^{4} yr
^{88}Nb $\rightarrow$ ^{88}Zr	EC	$1d_{5/2}$ - $1p_{3/2}$	7.43(5) $\times$ 10^{-6}	1.57 $\times$ 10^{-5}	5.83(4) $\times$ 10^{4}	90(20) yr
	β^+				4.58(5) $\times$ 10^{5}	11(3) yr
	EC/β^+				5.17(5) $\times$ 10^{5}	10(2) yr
^{88}Zr $\rightarrow$ ^{88}Y	EC	$1p_{3/2}$ - $1d_{5/2}$	4.09(3) $\times$ 10^{-6}	1.50 $\times$ 10^{-5}	1.6(2) $\times$ 10^{-4}	1.0(3) $\times$ 10^{11} yr
^{88}Y $\rightarrow$ ^{88}Sr	EC	$0h_{11/2}$ - $0g_{9/2}$	1.56(6) $\times$ 10^{-8}	1.58 $\times$ 10^{-5}	136(5)	7(2) $\times$ 10^{10} yr
	β^+				53(4)	1.9(4) $\times$ 10^{11} yr
	EC/β^+				189(8)	5(1) $\times$ 10^{10} yr
^{90}Mo $\rightarrow$ ^{90}Nb*	EC	$1p_{3/2}$ - $1d_{5/2}$	4.77(4) $\times$ 10^{-6}	1.51 $\times$ 10^{-5}	5.6(6)	2.2(6) $\times$ 10^{6} yr
	β^+				9(2) $\times$ 10^{-2}	1.3(4) $\times$ 10^{8} yr
	EC/β^+				5.7(6)	2.2(6) $\times$ 10^{6} yr
^{90}Nb* $\rightarrow$ ^{90}Zr	EC	$0h_{11/2}$ - $0g_{9/2}$	7.87(6) $\times$ 10^{-6}	1.65 $\times$ 10^{-5}	1.28(5) $\times$ 10^{4}	340(80) yr
	β^+				5.5(3) $\times$ 10^{4}	80(20) yr
	EC/β^+				6.7(4) $\times$ 10^{4}	70(20) yr
^{146}Gd $\rightarrow$ ^{146}Eu	EC	$1d_{5/2} - 2p_{3/2}$	1.54(6) $\times$ 10^{-5}	1.98 $\times$ 10^{-5}	2.8(2) $\times$ 10^{-2}	2.8(6) $\times$ 10^{12} yr
	β^+				9.8(9) $\times$ 10^{-17}	9(3) $\times$ 10^{21} yr
	EC/β^+				2.8(2) $\times$ 10^{-2}	2.8(6) $\times$ 10^{12} yr
^{146}Eu $\rightarrow$ ^{146}Sm	EC	$1d_{3/2}$ - $0h_{11/2}$	7.25(5) $\times$ 10^{-6}	2.57 $\times$ 10^{-5}	1.46(2) $\times$ 10^{3}	2.2(5) $\times$ 10^{4} yr
	β^+				92(2)	3.5(7) $\times$ 10^{5} yr
	EC/β^+				1.55(3) $\times$ 10^{3}	2.1(5) $\times$ 10^{4} yr

the reduction factor k amounts to

$$k = \frac{M_{\mathrm{pnQRPA}}}{M_{\mathrm{qp}}} = 0.29 \pm 0.15 \quad \text{(GROUP 1)}. \qquad (16)$$

For GROUP 2 there does not exist a meaningful value for k that could be assigned to the group as a whole. For approximately half of the decays in GROUP 2 the k value is exceptionally large, around 0.5–0.8. For the other half the k value is very low, less than 5×10^{-3}. Only a few decays have k values in the region 0.005–0.5, and for these the k value is relatively low compared to the decays in GROUP 1, between 0.008 and 0.15. Approximately half of the decays for each degree of forbiddenness have a very low k value. Only for third-forbidden decays are these low values not seen, but this is statistically insignificant since there are only three studied cases.

In Fig. 3 the NMEs of GROUP 1 fall roughly into three regions, with the mass ranges $A = 50$–88, $A = 90$–120, and $A = 122$–146. In the first region the k value appears to have a constant mean of 0.4, with a low variance. The k values of the second region seem to be more scattered, with the mean value slightly lower than in the first region, and the values decrease as the mass number increases. The third region has a lower mean than the first two regions, but the scattering is not so large. The factors k for these three regions, for each degree of forbiddenness, are listed in Table XI. For comparison, the second and third columns of the table include also the results of the earlier works [11] and [10] for the Gamow-Teller 1^+ and spin-dipole 2^- NMEs. The general trend for k is to decrease as A increases. The average reduction factors are $k = 0.39$, $k = 0.31$, and $k = 0.24$ for the first, second and third regions respectively. The reduction factor, however, is not a monotonic function of the degree of forbiddenness. The average values are slightly higher for the third- and fifth-forbidden than for the second- and fourth-forbidden decays, and for the seventh-forbidden decays the k value is the lowest. For the second- and fifth-forbidden decays the k value does not depend sensitively on the mass number, whereas in the third- and especially fourth-forbidden cases the reduction factor decreases significantly as A increases. The average of the reduction factors of the regions shown in the last line of Table XI was calculated to average out the effect of the different

TABLE VI. The same as Table IV for the fourth-forbidden unique $0^+ \leftrightarrow 5^+$ transitions.

Transition	Mode	p-n conf.	$\lvert M_{\mathrm{pnQRPA}}\rvert$ (fm^4)	$\lvert M_{\mathrm{qp}}\rvert$ (fm^4)	f	Expected $t_{1/2}$
^{50}Sc $\rightarrow$ ^{50}Ti	β^-	$1s_{1/2}$ - $0g_{9/2}$	8.13(5) $\times$ 10^{-8}	1.47 $\times$ 10^{-7}	5.7(2) $\times$ 10^{6}	8(2) $\times$ 10^{4} yr
^{50}Ca $\rightarrow$ ^{50}Sc	β^-	$1p_{3/2}$ - $0f_{7/2}$	1.11(4) $\times$ 10^{-7}	1.70 $\times$ 10^{-7}	1.04(4) $\times$ 10^{5}	2.1(5) $\times$ 10^{5} yr
^{50}Mn* $\rightarrow$ ^{50}Cr	EC	$1p_{3/2}$ - $0f_{7/2}$	7.32(5) $\times$ 10^{-8}	1.49 $\times$ 10^{-7}	4.36(1) $\times$ 10^{4}	1.3(3) $\times$ 10^{7} yr
	β^+				1.80(1) $\times$ 10^{6}	3.1(7) $\times$ 10^{5} yr
	EC/β^+				1.84(1) $\times$ 10^{6}	3.1(7) $\times$ 10^{5} yr
^{58}Co* $\rightarrow$ ^{58}Ni	β^-	$0f_{7/2}$ - $1p_{3/2}$	1.08(1) $\times$ 10^{-7}	1.44 $\times$ 10^{-7}	3.28(10) $\times$ 10^{-7}	8(2) $\times$ 10^{17} yr
^{58}Co* $\rightarrow$ ^{58}Fe	EC	$1p_{3/2}$ - $0f_{7/2}$	7.62(5) $\times$ 10^{-8}	1.86 $\times$ 10^{-7}	2.90(2) $\times$ 10^{-1}	1.8(4) $\times$ 10^{12} yr
	β^+				8.12(8) $\times$ 10^{-3}	6(2) $\times$ 10^{13} yr
	EC/β^+				2.98(2) $\times$ 10^{-1}	1.7(4) $\times$ 10^{12} yr
^{60}Fe $\rightarrow$ ^{60}Co	β^-	$1p_{3/2}$ - $0f_{7/2}$	7.98(6) $\times$ 10^{-8}	1.89 $\times$ 10^{-7}	2.7(4) $\times$ 10^{-9}	1.6(4) $\times$ 10^{19} yr
^{60}Co $\rightarrow$ ^{60}Ni	β^-	$1s_{1/2}$ - $0g_{9/2}$	9.39(7) $\times$ 10^{-8}	1.65 $\times$ 10^{-7}	171(1)	2.0(5) $\times$ 10^{9} yr
^{62}Fe $\rightarrow$ ^{62}Co*	β^-	$1p_{3/2}$ - $0f_{7/2}$	7.17(5) $\times$ 10^{-8}	1.93 $\times$ 10^{-7}	46.2(44)	1.2(4) $\times$ 10^{9} yr
^{62}Co* $\rightarrow$ ^{62}Ni	β^-	$1s_{1/2}$ - $0g_{9/2}$	5.70(22) $\times$ 10^{-11}	1.66 $\times$ 10^{-7}	3.12(15) $\times$ 10^{5}	3.0(6) $\times$ 10^{12} yr
^{98}Zr $\rightarrow$ ^{98}Nb*	β^-	$0h_{11/2}$ - $1p_{1/2}$	2.11(2) $\times$ 10^{-7}	3.20 $\times$ 10^{-7}	12.0(8)	1.1(3) $\times$ 10^{9} yr
^{98}Nb* $\rightarrow$ ^{98}Mo	β^-	$0g_{9/2} - 2s_{1/2}$	1.93(2) $\times$ 10^{-7}	2.78 $\times$ 10^{-7}	9.32(17) $\times$ 10^{4}	1.9(5) $\times$ 10^{6} yr
^{98}Pd $\rightarrow$ ^{98}Rh*	EC	$1p_{1/2}$ - $0h_{11/2}$	1.91(2) $\times$ 10^{-7}	2.99 $\times$ 10^{-7}	1.7(2) $\times$ 10^{-1}	9(3) $\times$ 10^{10} yr
	β^+				4.4(8) $\times$ 10^{-5}	3.7(9) $\times$ 10^{14} yr
	EC/β^+				1.7(2) $\times$ 10^{-1}	9(3) $\times$ 10^{10} yr
^{98}Rh* $\rightarrow$ ^{98}Ru	EC	$0h_{11/2}$ - $1p_{1/2}$	5.52(4) $\times$ 10^{-8}	3.20 $\times$ 10^{-7}	3.94(8) $\times$ 10^{3}	5(2) $\times$ 10^{8} yr
	β^+				2.08(7) $\times$ 10^{3}	1.0(3) $\times$ 10^{9} yr
	EC/β^+				6.0(2) $\times$ 10^{3}	3.5(8) $\times$ 10^{8} yr
^{100}Zr $\rightarrow$ ^{100}Nb*	β^-	$1d_{5/2}$ - $1d_{5/2}$	1.97(2) $\times$ 10^{-7}	3.97 $\times$ 10^{-7}	766(78)	2.0(6) $\times$ 10^{7} yr
^{100}Nb* $\rightarrow$ ^{100}Mo	β^-	$0f_{7/2}$ - $0h_{11/2}$	1.43(1) $\times$ 10^{-7}	2.49 $\times$ 10^{-7}	7.19(34) $\times$ 10^{6}	4.4(9) $\times$ 10^{4} yr
^{100}Cd $\rightarrow$ ^{100}Ag	EC	$1p_{1/2}$ - $0h_{11/2}$	2.02(2) $\times$ 10^{-8}	3.14 $\times$ 10^{-7}	415(6)	6(2) $\times$ 10^{8} yr
	β^+				45.0(10)	6(2) $\times$ 10^{9} yr
	EC/β^+				460(7)	5(2) $\times$ 10^{8} yr
^{100}Ag $\rightarrow$ ^{100}Pd	EC	$0h_{11/2}$ - $1p_{1/2}$	9.65(7) $\times$ 10^{-8}	3.24 $\times$ 10^{-7}	1.40(4) $\times$ 10^{5}	5(2) $\times$ 10^{6} yr
	β^+				2.79(11) $\times$ 10^{5}	2.5(6) $\times$ 10^{6} yr
	EC/β^+				4.19(14) $\times$ 10^{5}	1.7(4) $\times$ 10^{6} yr
^{100}Pd $\rightarrow$ ^{100}Rh*	EC	$1p_{1/2}$ - $0h_{11/2}$	1.72(2) $\times$ 10^{-8}	2.99 $\times$ 10^{-7}	1.29(20) $\times$ 10^{-10}	1.5(4) $\times$ 10^{22} yr
^{100}Rh* $\rightarrow$ ^{100}Ru	EC	$1d_{5/2}$ - $1d_{5/2}$	5.64(4) $\times$ 10^{-8}	3.65 $\times$ 10^{-7}	194(11)	1.0(2) $\times$ 10^{9} yr
	β^+				20.9(18)	9(2) $\times$ 10^{9} yr
	EC/β^+				214(12)	9(2) $\times$ 10^{8} yr
^{102}Cd $\rightarrow$ ^{102}Ag	EC	$1p_{1/2}$ - $0h_{11/2}$	1.81(2) $\times$ 10^{-7}	3.15 $\times$ 10^{-7}	5.9(2)	3.0(7) $\times$ 10^{9} yr
	β^+				3.7(3) $\times$ 10^{-2}	4.8(1) $\times$ 10^{11} yr
	EC/β^+				5.9(2)	3.0(7) $\times$ 10^{9} yr
^{102}Ag $\rightarrow$ ^{102}Pd	EC	$1d_{5/2}$ - $1d_{5/2}$	1.18(1) $\times$ 10^{-7}	3.60 $\times$ 10^{-7}	1.52(3) $\times$ 10^{4}	3.0(7) $\times$ 10^{7} yr
	β^+				1.16(3) $\times$ 10^{4}	4.0(9) $\times$ 10^{7} yr
	EC/β^+				2.67(6) $\times$ 10^{4}	1.7(4) $\times$ 10^{7} yr
^{104}Cd $\rightarrow$ ^{104}Ag	EC	$1p_{1/2}$ - $0h_{11/2}$	1.66(2) $\times$ 10^{-7}	3.16 $\times$ 10^{-7}	1.48(7) $\times$ 10^{-3}	1.4(3) $\times$ 10^{13} yr
	β^+				8(4) $\times$ 10^{-13}	3(2) $\times$ 10^{22} yr
	EC/β^+				1.48(7) $\times$ 10^{-3}	1.4(3) $\times$ 10^{13} yr
^{104}Ag $\rightarrow$ ^{104}Pd	EC	$1d_{5/2}$ - $1d_{5/2}$	1.41(1) $\times$ 10^{-7}	3.97 $\times$ 10^{-7}	872(9)	3.7(8) $\times$ 10^{8} yr
	β^+				163(3)	2.0(5) $\times$ 10^{9} yr
	EC/β^+				1.04(2) $\times$ 10^{4}	3.1(7) $\times$ 10^{8} yr
^{104}Rh* $\rightarrow$ ^{104}Ru	EC	$0h_{11/2}$ - $1p_{1/2}$	1.93(2) $\times$ 10^{-7}	3.33 $\times$ 10^{-7}	3.28(9) $\times$ 10^{-3}	5(2) $\times$ 10^{13} yr
	β^+				3.12(38) $\times$ 10^{-10}	6(2) $\times$ 10^{20} yr
	EC/β^+				3.28(9) $\times$ 10^{-3}	5(2) $\times$ 10^{13} yr
^{104}Rh* $\rightarrow$ ^{104}Pd	β^-	$1p_{1/2}$ - $0h_{11/2}$	1.97(2) $\times$ 10^{-7}	3.00 $\times$ 10^{-7}	102(2)	1.6(4) $\times$ 10^{9} yr
^{114}In* $\rightarrow$ ^{114}Cd	EC	$1d_{5/2}$ - $1d_{5/2}$	1.05(1) $\times$ 10^{-7}	4.61 $\times$ 10^{-7}	6.00(3) $\times$ 10^{-2}	1.0(2) $\times$ 10^{13} yr
	β^+				1.86(3) $\times$ 10^{-6}	3.1(6) $\times$ 10^{17} yr
	EC/β^+				6.00(3) $\times$ 10^{-2}	1.0(2) $\times$ 10^{13} yr
^{114}In* $\rightarrow$ ^{114}Sn	β^-	$1p_{3/2}$ - $1f_{7/2}$	7.61(29) $\times$ 10^{-10}	3.70 $\times$ 10^{-7}	18.4(1)	6(2) $\times$ 10^{9} yr

TABLE VII. The same as Table IV for the fourth-forbidden unique $0^+ \leftrightarrow 5^+$ transitions.

Transition	Mode	p-n conf.	$\lvert M_{\rm pnQRPA}\rvert$ (fm^7)	$\lvert M_{\rm qp}\rvert$ (fm^7)	f	Expected $t_{1/2}$
^{116}In$^* \rightarrow {}^{116}$Cd	EC	$1d_{5/2}$ - $1d_{5/2}$	$1.19(1) \times 10^{-7}$	4.70×10^{-7}	$1.53(1) \times 10^{-6}$	$3.0(6) \times 10^{17}$ yr
^{116}In$^* \rightarrow {}^{116}$Sn	β^-	$1p_{3/2}$ - $1f_{7/2}$	$4.52(18) \times 10^{-10}$	3.74×10^{-7}	$2.94(1) \times 10^{3}$	$1.1(3) \times 10^{13}$ yr
^{118}Cd $\rightarrow {}^{118}$In*	β^-	$1d_{5/2}$ - $1d_{5/2}$	$1.34(1) \times 10^{-7}$	4.72×10^{-7}	$2.7(14) \times 10^{-6}$	$1.2(5) \times 10^{16}$ yr
^{118}In$^* \rightarrow {}^{118}$Sn	β^-	$1p_{3/2}$ - $1f_{7/2}$	$2.85(11) \times 10^{-10}$	3.78×10^{-7}	$7.44(16) \times 10^{4}$	$1.1(3) \times 10^{12}$ yr
^{120}Cd $\rightarrow {}^{120}$In*	β^-	$1d_{5/2}$ - $1d_{5/2}$	$1.46(1) \times 10^{-7}$	4.82×10^{-7}	1.15(44)	$2.4(8) \times 10^{10}$ yr
^{120}In$^* \rightarrow {}^{120}$Sn	β^-	$1p_{3/2}$ - $1f_{7/2}$	$1.86(8) \times 10^{-13}$	3.81×10^{-7}	$7.4(9) \times 10^{5}$	$2.5(6) \times 10^{17}$ yr
^{122}Cd $\rightarrow {}^{122}$In*	β^-	$1d_{5/2}$ - $1d_{5/2}$	$1.58(2) \times 10^{-7}$	4.90×10^{-7}	175(42)	$1.3(4) \times 10^{8}$ yr
^{122}In$^* \rightarrow {}^{122}$Sn	β^-	$1p_{3/2}$ - $1f_{7/2}$	$3.27(13) \times 10^{-12}$	3.84×10^{-7}	$8.5(9) \times 10^{6}$	$7(2) \times 10^{13}$ yr
^{124}Sb$^* \rightarrow {}^{124}$Sn	EC	$0h_{11/2}$ - $1p_{1/2}$	$2.27(2) \times 10^{-8}$	3.70×10^{-7}	$2.55(10) \times 10^{-6}$	$5(2) \times 10^{18}$ yr
^{124}Sb$^* \rightarrow {}^{124}$Te	β^-	$1p_{3/2}$ - $1f_{7/2}$	$3.20(13) \times 10^{-9}$	3.85×10^{-7}	526(4)	$1.2(3) \times 10^{12}$ yr
^{126}Sn $\rightarrow {}^{126}$Sb*	β^-	$1d_{5/2}$ - $1d_{5/2}$	$2.55(9) \times 10^{-8}$	5.05×10^{-7}	2.95(1 mag) $\times 10^{-7}$	3(1 mag) $\times 10^{18}$ yr
^{126}Sb$^* \rightarrow {}^{126}$Te	β^-	$1p_{3/2}$ - $1f_{7/2}$	$3.51(14) \times 10^{-9}$	3.90×10^{-7}	$8.0(8) \times 10^{3}$	$7(2) \times 10^{10}$ yr
^{128}Sn $\rightarrow {}^{128}$Sb*	β^-	$1d_{5/2}$ - $1d_{5/2}$	$2.47(9) \times 10^{-8}$	5.13×10^{-7}	$5.4(7) \times 10^{-2}$	$1.8(4) \times 10^{13}$ yr
^{128}Sb$^* \rightarrow {}^{128}$Te	β^-	$1p_{3/2}$ - $1f_{7/2}$	$3.35(13) \times 10^{-9}$	3.93×10^{-7}	$57.2(4) \times 10^{4}$	$1.0(2) \times 10^{10}$ yr
^{130}I $\rightarrow {}^{130}$Te	EC	$1d_{5/2}$ - $1d_{5/2}$	$2.55(2) \times 10^{-8}$	4.86×10^{-7}	$4.3(4) \times 10^{-8}$	$2.3(6) \times 10^{20}$ yr
^{130}I $\rightarrow {}^{130}$Xe	β^-	$1p_{3/2}$ - $1f_{7/2}$	$4.60(3) \times 10^{-9}$	3.96×10^{-7}	630(8)	$5(1) \times 10^{11}$ yr
^{136}Cs $\rightarrow {}^{136}$Xe	EC	$1d_{5/2}$ - $1d_{5/2}$	$7.55(29) \times 10^{-10}$	4.82×10^{-7}	$5.2(27) \times 10^{-17}$	$2.2(8) \times 10^{32}$ yr
^{136}Cs $\rightarrow {}^{136}$Ba	β^-	$1p_{3/2}$ - $1f_{7/2}$	$3.63(2) \times 10^{-9}$	4.08×10^{-7}	131(12)	$4(1) \times 10^{12}$ yr
^{138}La $\rightarrow {}^{138}$Ba	EC	$0h_{11/2}$ - $0h_{11/2}$	$1.14(5) \times 10^{-9}$	4.70×10^{-7}	$1.91(4) \times 10^{-1}$	$8(2) \times 10^{15}$ yr
	β^+				$7.8(4) \times 10^{-6}$	$2.0(5) \times 10^{20}$ yr
	EC/β^+				$1.91(4) \times 10^{-1}$	$8(2) \times 10^{15}$ yr
^{138}La $\rightarrow {}^{138}$Ce	β^-	$1p_{1/2}$ - $1f_{7/2}$	$4.66(3) \times 10^{-9}$	4.11×10^{-7}	$1.0(1) \times 10^{-2}$	$9(3) \times 10^{15}$ yr

TABLE VIII. The same as Table IV for the fifth-forbidden unique $0^+ \leftrightarrow 6^-$ transitions.

Transition	Mode	p-n conf.	$\lvert M_{\rm pnQRPA}\rvert$ (fm^5)	$\lvert M_{\rm qp}\rvert$ (fm^5)	f	Expected $t_{1/2}$
^{84}Se $\rightarrow {}^{84}$Br*	β^-	$0h_{11/2}$ - $0g_{9/2}$	$3.27(3) \times 10^{-11}$	5.89×10^{-9}	$1.5(5) \times 10^{-2}$	$1.7(8) \times 10^{19}$ yr
^{84}Br$^* \rightarrow {}^{84}$Kr	β^-	$0f_{7/2}$ - $1d_{5/2}$	$1.79(2) \times 10^{-9}$	5.04×10^{-9}	$9.8(9) \times 10^{4}$	$1.1(3) \times 10^{10}$ yr
^{84}Rb$^* \rightarrow {}^{84}$Kr	EC	$0g_{9/2}$ - $1p_{3/2}$	$2.31(2) \times 10^{-9}$	5.53×10^{-9}	5.16(7)	$1.3(3) \times 10^{14}$ yr
	β^+				$1.76(4) \times 10^{-1}$	$3.8(7) \times 10^{15}$ yr
	EC/β^+				5.33(7)	$1.3(3) \times 10^{14}$ yr
^{84}Rb$^* \rightarrow {}^{84}$Sr	β^-	$0f_{7/2}$ - $1d_{5/2}$	$2.90(2) \times 10^{-9}$	5.05×10^{-9}	$4.00(9) \times 10^{-3}$	$1.1(3) \times 10^{17}$ yr
^{86}Rb$^* \rightarrow {}^{86}$Kr	EC	$0h_{11/2}$ - $0g_{9/2}$	$5.48(21) \times 10^{-12}$	5.99×10^{-9}	$1.14(1) \times 10^{-5}$	$1.0(4) \times 10^{25}$ yr
	β^+				$7.3(3) \times 10^{-19}$	$1.6(4) \times 10^{38}$ yr
	EC/β^+				$1.14(1) \times 10^{-5}$	$1.0(4) \times 10^{25}$ yr
^{86}Rb$^* \rightarrow {}^{86}$Sr	β^-	$0f_{7/2}$ - $1d_{5/2}$	$2.09(2) \times 10^{-9}$	5.11×10^{-9}	3.90(3)	$2.1(5) \times 10^{14}$ yr
^{120}Pd $\rightarrow {}^{120}$Ag*	β^-	$1f_{7/2}$ - $1d_{5/2}$	$3.06(2) \times 10^{-9}$	1.26×10^{-8}	$2.26(4) \times 10^{5}$	$2.8(7) \times 10^{8}$ yr
^{120}Ag$^* \rightarrow {}^{120}$Cd	β^-	$0g_{9/2} - 2p_{3/2}$	$4.65(3) \times 10^{-9}$	7.57×10^{-9}	$2.52(26) \times 10^{8}$	$1.4(4) \times 10^{6}$ yr
^{132}Ce $\rightarrow {}^{132}$La*	EC	$0g_{9/2} - 2p_{3/2}$	$2.84(2) \times 10^{-9}$	8.81×10^{-9}	$4.0(17) \times 10^{-5}$	$1.8(7) \times 10^{18}$ yr
	β^+				3(3 mag) $\times 10^{-20}$	2(3 mag) $\times 10^{33}$ yr
	EC/β^+				$4.0(17) \times 10^{-5}$	$1.8(7) \times 10^{18}$ yr
^{132}La$^* \rightarrow {}^{132}$Ba	EC	$1f_{7/2}$ - $1d_{5/2}$	$6.49(5) \times 10^{-9}$	1.37×10^{-8}	$5.3(6) \times 10^{3}$	$3.4(8) \times 10^{10}$ yr
	β^+				390(70)	$5(2) \times 10^{11}$ yr
	EC/β^+				$5.7(7) \times 10^{3}$	$3.2(8) \times 10^{10}$ yr
^{134}Nd $\rightarrow {}^{134}$Pr	EC	$0g_{9/2} - 2p_{3/2}$	$3.46(3) \times 10^{-9}$	8.90×10^{-9}	10.3(12)	$5(1) \times 10^{12}$ yr
	β^+				$2.1(4) \times 10^{-2}$	$2.3(7) \times 10^{15}$ yr
	EC/β^+				10.3(12)	$5(1) \times 10^{12}$ yr
^{134}Pr $\rightarrow {}^{134}$Ce	EC	$1f_{7/2}$ - $1d_{5/2}$	$6.41(5) \times 10^{-9}$	1.37×10^{-8}	$1.28(8) \times 10^{5}$	$1.4(4) \times 10^{9}$ yr
	β^+				$2.72(23) \times 10^{4}$	$7(2) \times 10^{9}$ yr
	EC/β^+				$1.56(10) \times 10^{5}$	$1.2(3) \times 10^{9}$ yr
^{136}Te $\rightarrow {}^{136}$I*	β^-	$1f_{7/2}$ - $1d_{5/2}$	$3.16(3) \times 10^{-9}$	1.42×10^{-8}	$3.81(22) \times 10^{4}$	$1.5(5) \times 10^{9}$ yr
^{136}I$^* \rightarrow {}^{136}$Xe	β^-	$0g_{9/2} - 2p_{3/2}$	$5.56(4) \times 10^{-9}$	9.09×10^{-9}	$5.29(2) \times 10^{8}$	$5(1) \times 10^{6}$ yr
^{138}Xe $\rightarrow {}^{138}$Cs*	β^-	$1f_{7/2}$ - $1d_{5/2}$	$5.12(3) \times 10^{-9}$	1.43×10^{-8}	87(5)	$8(3) \times 10^{10}$ yr
^{138}Cs$^* \rightarrow {}^{138}$Ba	β^-	$0g_{9/2} - 2p_{3/2}$	$7.00(5) \times 10^{-9}$	9.17×10^{-9}	$6.30(2) \times 10^{5}$	$6(2) \times 10^{6}$ yr

TABLE IX. The same as Table IV for the sixth-forbidden unique $0^+ \leftrightarrow 7^+$ transitions.

Transition	Mode	p-n conf.	$\lvert M_{\mathrm{pnQRPA}}\rvert$ (fm^6)	$\lvert M_{\mathrm{qp}}\rvert$ (fm^6)	f	Expected $t_{1/2}$
^{54}Co* $\rightarrow$ ^{54}Fe	EC	$0d_{5/2}$ - $0g_{9/2}$	1.32(6) $\times$ 10^{-13}	4.71 $\times$ 10^{-11}	1.34(1) $\times$ 10^{6}	1.8(4) $\times$ 10^{17} yr
	β^+				7.10(1) $\times$ 10^{6}	3.3(7) $\times$ 10^{16} yr
	EC/β^+				8.45(1) $\times$ 10^{6}	2.8(6) $\times$ 10^{16} yr
^{54}Ni $\rightarrow$ ^{54}Co*	EC	$0g_{9/2}$ - $0d_{5/2}$	7.21(26) $\times$ 10^{-14}	4.71 $\times$ 10^{-11}	1.94(17) $\times$ 10^{6}	2.7(6) $\times$ 10^{16} yr
	β^+				9.6(11) $\times$ 10^{6}	5(2) $\times$ 10^{15} yr
	EC/β^+				1.15(13) $\times$ 10^{7}	5(1) $\times$ 10^{15} yr
^{92}Nb $\rightarrow$ ^{92}Zr	EC	$1d_{5/2}$ - $0g_{9/2}$	7.03(5) $\times$ 10^{-11}	1.56 $\times$ 10^{-10}	9.14(12) $\times$ 10^{-3}	9(2) $\times$ 10^{19} yr
	β^+				3.89(10) $\times$ 10^{-7}	2.1(3) $\times$ 10^{24} yr
	EC/β^+				9.14(12) $\times$ 10^{-3}	9(2) $\times$ 10^{19} yr
^{92}Nb $\rightarrow$ ^{92}Mo	β^-	$1p_{3/2}$ - $0h_{11/2}$	8.79(6) $\times$ 10^{-11}	1.42 $\times$ 10^{-10}	1.26(11) $\times$ 10^{-11}	4(1) $\times$ 10^{28} yr
^{94}Ru $\rightarrow$ ^{94}Tc	EC	$1p_{3/2}$ - $0h_{11/2}$	1.08(4) $\times$ 10^{-13}	1.46 $\times$ 10^{-10}	3.7(2) $\times$ 10^{-4}	6(2) $\times$ 10^{25} yr
	β^+				2.1(3) $\times$ 10^{-10}	1.1(3) $\times$ 10^{32} yr
	EC/β^+				3.7(2) $\times$ 10^{-4}	6(2) $\times$ 10^{25} yr
^{94}Tc $\rightarrow$ ^{94}Mo	EC	$1d_{5/2}$ - $0g_{9/2}$	5.95(4) $\times$ 10^{-11}	1.59 $\times$ 10^{-10}	442(6)	2.6(6) $\times$ 10^{15} yr
	β^+				10.9(3)	1.1(3) $\times$ 10^{17} yr
	EC/β^+				453(7)	2.5(6) $\times$ 10^{15} yr
^{96}Tc $\rightarrow$ ^{96}Mo	EC	$1d_{5/2}$ - $0g_{9/2}$	8.63(6) $\times$ 10^{-11}	1.62 $\times$ 10^{-10}	2.81(7)	2.0(5) $\times$ 10^{17} yr
	β^+				5.6(3) $\times$ 10^{-3}	1.0(3) $\times$ 10^{20} yr
	EC/β^+				2.81(7)	2.0(5) $\times$ 10^{17} yr
^{96}Tc $\rightarrow$ ^{96}Ru	β^-	$1p_{3/2}$ - $0h_{11/2}$	9.39(7) $\times$ 10^{-11}	1.47 $\times$ 10^{-10}	4(2) $\times$ 10^{-13}	1.1(4) $\times$ 10^{30} yr
^{106}Sn $\rightarrow$ ^{106}In	EC	$1p_{3/2}$ - $0h_{11/2}$	1.17(35) $\times$ 10^{-10}	1.64 $\times$ 10^{-10}	17.2(11)	2.5(6) $\times$ 10^{15} yr
	β^+				3.58(33) $\times$ 10^{-2}	1.2(3) $\times$ 10^{18} yr
	EC/β^+				17.3(11)	2.5(6) $\times$ 10^{15} yr
^{106}In $\rightarrow$ ^{106}Cd	EC	$1d_{5/2}$ - $0g_{9/2}$	1.29(1) $\times$ 10^{-10}	1.77 $\times$ 10^{-10}	2.92(8) $\times$ 10^{5}	1.9(4) $\times$ 10^{12} yr
	β^+				3.96(14) $\times$ 10^{4}	1.4(3) $\times$ 10^{13} yr
	EC/β^+				3.31(10) $\times$ 10^{5}	1.7(4) $\times$ 10^{12} yr
^{108}Sn $\rightarrow$ ^{108}In	EC	$1p_{3/2}$ - $0h_{11/2}$	9.72(5) $\times$ 10^{-11}	1.67 $\times$ 10^{-10}	2.4(2) $\times$ 10^{-2}	2.6(7) $\times$ 10^{18} yr
	β^+				5.9(9) $\times$ 10^{-7}	1.1(3) $\times$ 10^{23} yr
	EC/β^+				2.4(2) $\times$ 10^{-2}	2.6(7) $\times$ 10^{18} yr
^{108}In $\rightarrow$ ^{108}Cd	EC	$1d_{5/2}$ - $0g_{9/2}$	6.31(24) $\times$ 10^{-11}	1.79 $\times$ 10^{-10}	1.0(3) $\times$ 10^{4}	2.2(5) $\times$ 10^{14} yr
	β^+				403(14)	5(2) $\times$ 10^{15} yr
	EC/β^+				1.0(3) $\times$ 10^{4}	2.2(5) $\times$ 10^{14} yr
^{110}Sn $\rightarrow$ ^{110}In	EC	$1p_{3/2}$ - $0h_{11/2}$	8.75(4) $\times$ 10^{-11}	1.66 $\times$ 10^{-10}	9(6) $\times$ 10^{-10}	9(6) $\times$ 10^{25} yr
^{110}In $\rightarrow$ ^{110}Cd	EC	$1d_{5/2}$ - $0g_{9/2}$	6.27(5) $\times$ 10^{-11}	1.83 $\times$ 10^{-10}	191(9)	1.2(3) $\times$ 10^{16} yr
	β^+				1.5(1)	1.5(4) $\times$ 10^{18} yr
	EC/β^+				192(9)	1.2(3) $\times$ 10^{16} yr

numbers of representative cases inside each mass region. This gives a meaningful k for the whole mass range $A = 50$–146 to be compared with the results of the earlier works on the allowed and first-forbidden transitions.

Even though k is not a smooth function of A, there are a few interesting smaller patterns in Figs. 3 and 4. In Fig. 3 there is a clear increasing linear behavior for the seventh-forbidden decays for $A = 118$–126 and a decreasing one for $A = 126$–132. These are all β^- decays where the p-n configuration giving the largest contribution to the NME is $0h_{11/2}$ - $1d_{5/2}$. Another similar pattern is seen for the fourth-forbidden decays with $A = 114$–122. These are both β^+/EC and β^- decays with the main contributing p-n configuration being $1d_{5/2}$ - $1d_{5/2}$. In Fig. 4 there are also structured patterns for the seventh-forbidden $\beta^\pm$ decays, the main contributing p-n configuration being $0g_{9/2}$ - $1f_{7/2}$. Regularities of similar range are not seen for transitions of other degrees of forbiddenness. For example the k values for the second-forbidden β^+/EC decays ^{110,112,114,116}Te $\rightarrow$ Sb do not follow a clear pattern even though the dominating p-n configuration in the NMEs is $0f_{5/2}$ - $0h_{11/2}$ for all of these decays.

The fact that these patterns include both β^+ and β^- transitions suggests that there is no difference in the behavior of the NMEs of these two decay types, at least for the cases where the β^+ decay feeds to 0^+ ground state of the even-even nucleus. To verify this we have investigated the values of k separately for the β^+/EC and β^- decays. The results are given in Figs. 6 and 7. Visibly in the figures the k values do not seem to behave any way differently for the β^+/EC and β^- decays.

The effect of Pauli blocking on β^+/EC decays is well know for the allowed Gamow-Teller transitions. This blocking grows stronger for heavy nuclei and further away from the stability line towards the neutron-rich side of the nuclear chart. In the present case of highly forbidden β transitions the Pauli blocking is caused by the factor $v_p u_n$ present in the one-body transition density (11). The effect of Pauli blocking can be examined by recording the values of the $v_p u_n$ factors as functions of mass number A in the case of $0^+_{\mathrm{gs}} \rightarrow J^\pi$

TABLE X. The same as Table IV for the seventh-forbidden unique $0^+ \leftrightarrow 8^-$ transitions.

Transition	Mode	p-n conf.	$\lvert M_{\mathrm{pnQRPA}}\rvert$ (fm^7)	$\lvert M_{\mathrm{qp}}\rvert$ (fm^7)	f	Expected $t_{1/2}$
^{116}Te $\rightarrow$ ^{116}Sb*	EC	$1d_{5/2}$ - $0h_{11/2}$	2.54(2) $\times$ 10^{-13}	5.26 $\times$ 10^{-12}	4(2) $\times$ 10^{-5}	2(1) $\times$ 10^{26} yr
	β^+				1.11(15) $\times$ 10^{-17}	8(3) $\times$ 10^{38} yr
	EC/β^+				4(2) $\times$ 10^{-5}	2(1) $\times$ 10^{26} yr
^{116}Sb* $\rightarrow$ ^{116}Sn	EC	$0g_{9/2}$ - $1f_{7/2}$	3.50(14) $\times$ 10^{-15}	5.11 $\times$ 10^{-12}	8.94(15) $\times$ 10^{5}	5(2) $\times$ 10^{19} yr
	β^+				3.95(9) $\times$ 10^{3}	1.2(3) $\times$ 10^{22} yr
	EC/β^+				8.98(15) $\times$ 10^{5}	5(2) $\times$ 10^{19} yr
^{116}In* $\rightarrow$ ^{116}Cd	EC	$0h_{11/2}$ - $1d_{5/2}$	6.99(5) $\times$ 10^{-13}	5.38 $\times$ 10^{-12}	2.18(2) $\times$ 10^{-8}	9(2) $\times$ 10^{29} yr
^{116}In* $\rightarrow$ ^{116}Sn	β^-	$0g_{9/2}$ - $1f_{7/2}$	3.50(14) $\times$ 10^{-15}	5.11 $\times$ 10^{-12}	5.51(1) $\times$ 10^{3}	1.5(4) $\times$ 10^{23} yr
^{118}Cd $\rightarrow$ ^{118}In*	β^-	$0h_{11/2}$ - $1d_{5/2}$	8.76(6) $\times$ 10^{-13}	5.45 $\times$ 10^{-12}	3.12(1 mag) $\times$ 10^{-12}	2(1 mag) $\times$ 10^{32} yr
^{118}In* $\rightarrow$ ^{118}Sn	β^-	$0g_{9/2}$ - $13_{7/2}$	4.06(16) $\times$ 10^{-15}	5.17 $\times$ 10^{-12}	5.07(16) $\times$ 10^{5}	2.7(5) $\times$ 10^{20} yr
^{120}Cd $\rightarrow$ ^{120}In*	β^-	$0h_{11/2}$ - $1d_{5/2}$	9.86(7) $\times$ 10^{-13}	5.59 $\times$ 10^{-12}	4.34(14) $\times$ 10^{-2}	1.4(3) $\times$ 10^{22} yr
^{120}In* $\rightarrow$ ^{120}Sn	β^-	$0g_{9/2}$ - $13_{7/2}$	5.45(21) $\times$ 10^{-15}	5.28 $\times$ 10^{-12}	7.02(10) $\times$ 10^{6}	5(1) $\times$ 10^{19} yr
^{120}Sb* $\rightarrow$ ^{120}Sn	EC	$0h_{11/2}$ - $1d_{5/2}$	2.77(2) $\times$ 10^{-12}	5.69 $\times$ 10^{-12}	28.5(13)	2.9(6) $\times$ 10^{19} yr
	β^+				1.25(9) $\times$ 10^{-3}	7(2) $\times$ 10^{23} yr
	EC/β^+				28.5(13)	2.9(6) $\times$ 10^{19} yr
^{120}Sb* $\rightarrow$ ^{120}Te	β^-	$0g_{9/2}$ - $1f_{7/2}$	2.84(11) $\times$ 10^{-12}	4.81 $\times$ 10^{-12}	3.6(5) $\times$ 10^{-6}	3(1) $\times$ 10^{26} yr
^{122}Cd $\rightarrow$ ^{122}In*	β^-	$0h_{11/2}$ - $1d_{5/2}$	1.10(1) $\times$ 10^{-12}	5.74 $\times$ 10^{-12}	38(15)	1.3(7) $\times$ 10^{19} yr
^{122}In* $\rightarrow$ ^{122}Sn	β^-	$0g_{9/2}$ - $1f_{7/2}$	3.07(12) $\times$ 10^{-15}	5.37 $\times$ 10^{-12}	3.2(5) $\times$ 10^{8}	3(2) $\times$ 10^{18} yr
^{122}Sb* $\rightarrow$ ^{122}Sn	EC	$0h_{11/2}$ - $1d_{5/2}$	3.49(3) $\times$ 10^{-12}	5.79 $\times$ 10^{-12}	3.38(13) $\times$ 10^{-2}	2.4(5) $\times$ 10^{22} yr
	β^+				1.03(8) $\times$ 10^{-8}	8(2) $\times$ 10^{28} yr
	EC/β^+				3.38(13) $\times$ 10^{-2}	2.4(5) $\times$ 10^{22} yr
^{122}Sb* $\rightarrow$ ^{122}Te	β^-	$0g_{9/2}$ - $1f_{7/2}$	1.74(2) $\times$ 10^{-12}	5.35 $\times$ 10^{-12}	1.10(3)	3.0(6) $\times$ 10^{21} yr
^{124}Cd $\rightarrow$ ^{124}In*	β^-	$0h_{11/2}$ - $1d_{5/2}$	1.21(1) $\times$ 10^{-12}	5.88 $\times$ 10^{-12}	6.5(9) $\times$ 10^{4}	6(2) $\times$ 10^{15} yr
^{124}In* $\rightarrow$ ^{124}Sn	β^-	$0g_{9/2}$ - $1f_{7/2}$	1.17(5) $\times$ 10^{-15}	5.45 $\times$ 10^{-12}	2.16(17) $\times$ 10^{9}	3.4(8) $\times$ 10^{18} yr
^{124}Sb* $\rightarrow$ ^{124}Sn	EC	$0h_{11/2}$ - $1d_{5/2}$	4.13(3) $\times$ 10^{-12}	5.90 $\times$ 10^{-12}	2.02(12) $\times$ 10^{-9}	2.9(8) $\times$ 10^{29} yr
^{124}Sb* $\rightarrow$ ^{124}Te	β^-	$0g_{9/2}$ - $1f_{7/2}$	1.44(1) $\times$ 10^{-12}	5.41 $\times$ 10^{-12}	218(3)	2.2(5) $\times$ 10^{19} yr
^{126}Sn $\rightarrow$ ^{126}Sb	β^-	$0h_{11/2}$ - $1d_{5/2}$	4.76(17) $\times$ 10^{-12}	5.98 $\times$ 10^{-12}	1.71(3) $\times$ 10^{4}	1.5(4) $\times$ 10^{15} yr
^{126}Sb $\rightarrow$ ^{126}Te	β^-	$0g_{9/2}$ - $1f_{7/2}$	1.25(1) $\times$ 10^{-12}	5.50 $\times$ 10^{-12}	9.7(15) $\times$ 10^{3}	7(2) $\times$ 10^{17} yr
^{128}Sn $\rightarrow$ ^{128}Sb	β^-	$0h_{11/2}$ - $1d_{5/2}$	5.11(18) $\times$ 10^{-12}	6.13 $\times$ 10^{-12}	2.5(5) $\times$ 10^{-4}	9(3) $\times$ 10^{22} yr
^{128}Sb $\rightarrow$ ^{128}Te	β^-	$0g_{9/2}$ - $1f_{7/2}$	1.02(1) $\times$ 10^{-12}	5.60 $\times$ 10^{-12}	1.96(16) $\times$ 10^{5}	5(2) $\times$ 10^{16} yr
^{130}Sn $\rightarrow$ ^{130}Sb	β^-	$0h_{11/2}$ - $1d_{5/2}$	5.04(18) $\times$ 10^{-12}	6.26 $\times$ 10^{-12}	1.13(13)	2.0(5) $\times$ 10^{19} yr
^{130}Sb $\rightarrow$ ^{130}Te	β^-	$0g_{9/2}$ - $1f_{7/2}$	7.85(6) $\times$ 10^{-13}	5.69 $\times$ 10^{-12}	2.71(14) $\times$ 10^{6}	6(2) $\times$ 10^{15} yr
^{132}Sn $\rightarrow$ ^{132}Sb	β^-	$0h_{11/2}$ - $1d_{5/2}$	2.99(11) $\times$ 10^{-12}	6.41 $\times$ 10^{-12}	493(12)	1.3(3) $\times$ 10^{17} yr
^{132}Sb $\rightarrow$ ^{132}Te	β^-	$0g_{9/2}$ - $1f_{7/2}$	4.92(4) $\times$ 10^{-13}	5.80 $\times$ 10^{-12}	1.36(2) $\times$ 10^{7}	2.8(6) $\times$ 10^{15} yr
^{134}Te $\rightarrow$ ^{134}I*	β^-	$0h_{11/2}$ - $1d_{5/2}$	4.90(18) $\times$ 10^{-12}	6.39 $\times$ 10^{-12}	1.24(10) $\times$ 10^{-4}	2.0(5) $\times$ 10^{23} yr
^{134}I* $\rightarrow$ ^{134}Xe	β^-	$0g_{9/2}$ - $1f_{7/2}$	8.07(6) $\times$ 10^{-13}	5.85 $\times$ 10^{-12}	2.28(6) $\times$ 10^{5}	7(2) $\times$ 10^{16} yr
^{134}Cs* $\rightarrow$ ^{134}Xe	EC	$0h_{11/2}$ - $1d_{5/2}$	5.30(4) $\times$ 10^{-12}	6.35 $\times$ 10^{-12}	6.41(7) $\times$ 10^{-4}	6(2) $\times$ 10^{23} yr
	β^+				4.16(13) $\times$ 10^{-13}	9(2) $\times$ 10^{32} yr
	EC/β^+				6.41(7) $\times$ 10^{-4}	6(2) $\times$ 10^{23} yr
^{134}Cs* $\rightarrow$ ^{134}Ba	β^-	$0g_{9/2}$ - $1f_{7/2}$	1.46(1) $\times$ 10^{-12}	5.85 $\times$ 10^{-12}	1.89(1)	2.5(5) $\times$ 10^{21} yr
^{136}Cs* $\rightarrow$ ^{136}Xe	EC	$0h_{11/2}$ - $1d_{5/2}$	1.54(6) $\times$ 10^{-15}	6.48 $\times$ 10^{-12}	7.4(5) $\times$ 10^{-10}	6(2) $\times$ 10^{36} yr
^{136}Cs* $\rightarrow$ ^{136}Ba	β^-	$0g_{9/2}$ - $1f_{7/2}$	9.94(65) $\times$ 10^{-13}	5.95 $\times$ 10^{-12}	514(6)	2.0(5) $\times$ 10^{19} yr

transitions. The results are presented in Fig. 8. It appears that the blocking increases, on average, with A as for the Gamow-Teller transitions. However, the blocking is not very strong due to the fact that all the presently discussed nuclei are very close to the bottom of the beta-stability line. Thus the

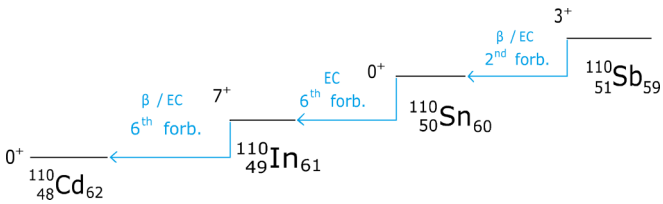

FIG. 1. A decay chain including some of the studied $A = 110$ nuclei.

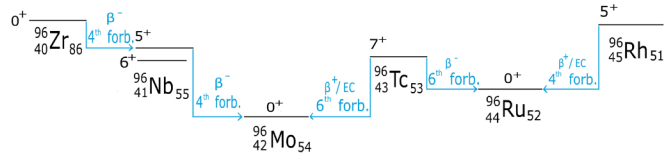

FIG. 2. A decay chain including some of the studied $A = 96$ nuclei.

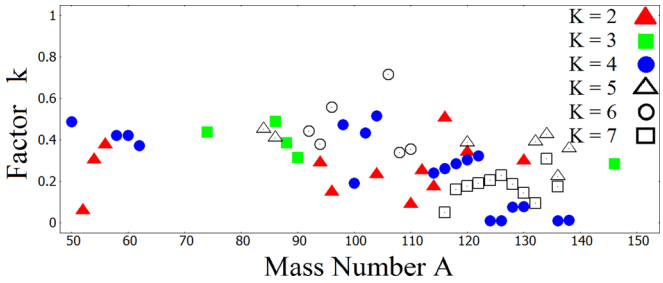

FIG. 3. Ratio $k = M_{\mathrm{pnQRPA}}/M_{\mathrm{qp}}$ as a function of mass the number A for transitions involving only nonmagic reference nuclei. The degree of forbiddenness K is marked by color and shape. For mass numbers with several calculated transitions the geometric mean, defined in Eq. (14), was used as the value of k.

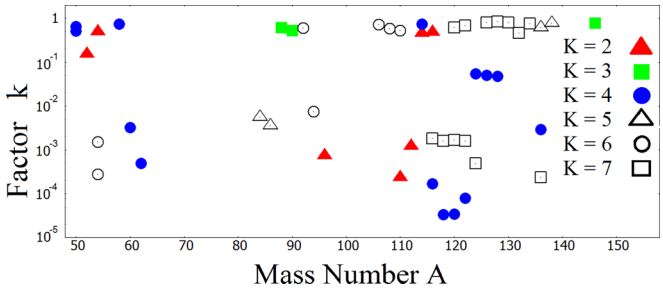

FIG. 4. Ratio $k = M_{\mathrm{pnQRPA}}/M_{\mathrm{qp}}$ as a function of the mass number A for transitions involving semimagic and magic reference nuclei. The k value of the transition $^{132}\mathrm{Sn}(0^+) \rightarrow {}^{132}\mathrm{Sb}^*(3^+)$ is cut off since it is much smaller than the other ones, at 1.15×10^{-7}. Note the logarithmic scale of the vertical axis.

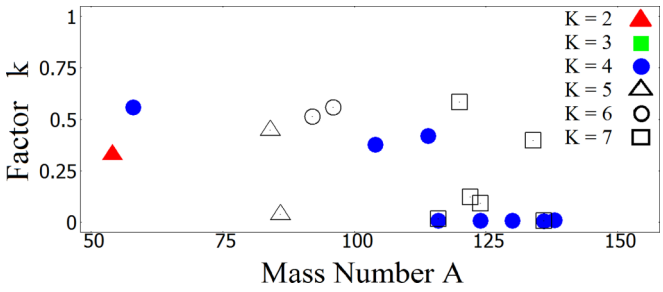

FIG. 5. Geometric mean of the ratio $k = M_{\mathrm{pnQRPA}}/M_{\mathrm{qp}}$ of the $\beta^{\pm}$ decay NMEs with a common mother or daughter nucleus. The symbol coding of Fig. 3 is used.

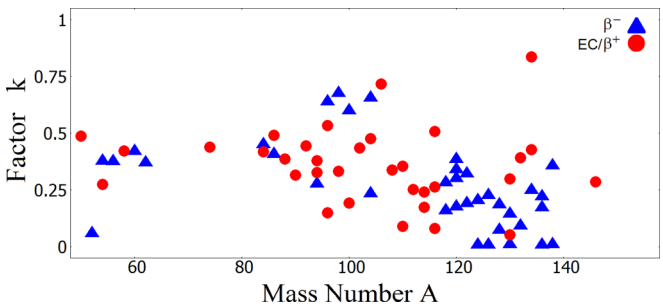

FIG. 6. Same as Fig. 3 but with the k values calculated separately for the β^+/EC and β^- decays. Note that the color/shape coding is not the one of Fig. 3.

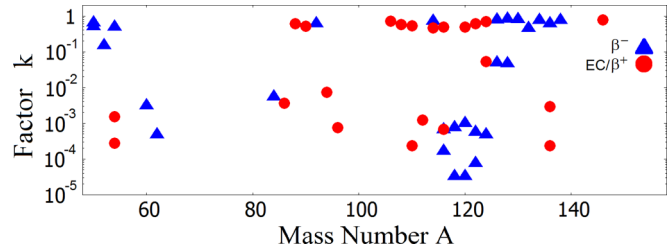

FIG. 7. Same as Fig 4 but with the k values calculated separately for the β^+/EC and β^- decays. Note that the color/shape coding is not the one of Fig. 4.

aspect of growing blocking when going towards neutron-rich nuclei is missing in the present calculations.

In GROUP 2 the differences in the k values of decays with neighboring reference nuclei can be several orders of magnitude. What makes the tin isotopes interesting is that for the second-forbidden transitions (see Table IV), in the case of the β^+ decay, the value of k for the decay involving the isotope ^{112}Sn ($k = 0.0011$) is much lower than for the other $A = 110, 114, 116$ tins. In [10], regarding the SD 2^- NMEs, the decays involving the semi-magic nuclei ^{86}Kr, ^{88}Sr, and ^{122}Sn were included in the study, but the ratios for them did not differ noticeably from the rest. This is commensurate with the above list of large-k semimagic cases for the second-forbidden transitions. For the very highly forbidden cases, 4th-, 6th-, and 7th-forbidden in Tables VI, IX, and X, all the tin-related transitions for the 6th-forbidden and the transitions containing low-mass ($A \leqslant 122$) tins in the 4th- and 7th-forbidden cases have rather large values of k. On the other hand, the 4th- and 7th-forbidden transitions for the heavier tins ($A \geqslant 122$) have quite small ratios k.

The strong division of the semimagic, (mostly) tin-related, transitions to the above-discussed cases of rather large and quite small k values relates to different ground-state configurations, different densities of the single-particle states at the proton and neutron Fermi surfaces, and the resulting differences in the BCS-based occupation and vacancy amplitudes. The NMEs of semi-magic nuclei are very sensitive to the single-particle energies, in particular of (few) key single-particle orbital(s). For a closer scrutiny of this effect, the

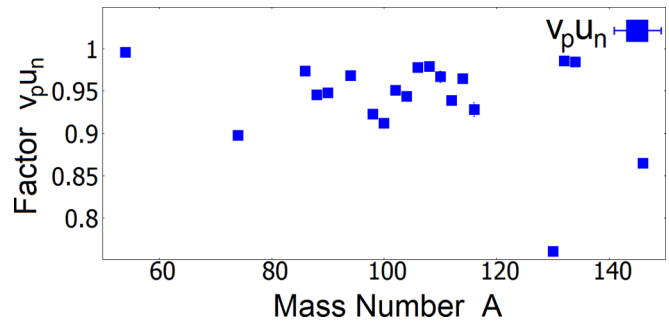

FIG. 8. Product of the proton occupation amplitude v_p and neutron vacancy amplitude u_n used for the calculation of the two-qp and pnQRPA nuclear matrix elements of β^+/EC $0^+_{\mathrm{gs}} \rightarrow J^\pi$ transitions as a function of the mass number.

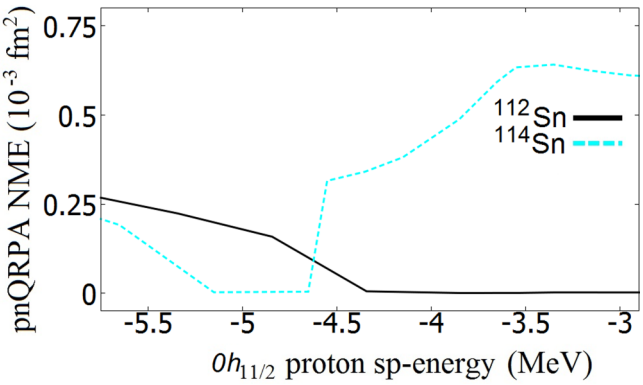

FIG. 9. The NMEs given by pnQRPA as functions of the single-particle energy of the $0h_{11/2}$ proton orbital for ^{112}Sn and ^{114}Sn.

single-particle energy of the proton orbital $0h_{11/2}$ was varied to see the effect on the second-forbidden pnQRPA NMEs of ^{112}Sn and ^{114}Sn. As seen in Table IV, this is a key orbital, along with the neutron $0f_{5/2}$ orbital, for all the cases involving a tin isotope within the mass range $110 \leqslant A \leqslant 116$. The results are presented in Fig 9. The behavior of the NMEs is similar for low single-particle energies, but there is a critical point at -4.7 MeV at which the pnQRPA NME of ^{114}Sn grows by two orders of magnitude.

The critical point is the single-particle energy at which the ground-state proton-neutron configuration changes from the $0g_{9/2}$ - $0g_{7/2}$ dominated at the lower energies to the $1d_{5/2}$ - $2s_{1/2}$ dominated at the higher energies of the $0h_{11/2}$ proton orbital. The energies of the proton orbital used for the calculations were -3.8 and -3.85 MeV for the ^{112}Sn and ^{114}Sn isotopes respectively, which are on the right side of the critical point. In the ^{110,116}Sn isotopes the dominant configuration is the same as in the ^{114}Sn isotope, resulting in a pnQRPA NME which is relatively large.

In the calculation of NMEs and half-lives presented in tables IV–X the values $g_{pp} = g_{ph} = 1.00$ were adopted for the scaling parameters. These calculations were done in a model space which assumed an inert core. We call these bases "small" in what follows. For nuclei with mass number $A = 50$–60 the core was chosen to consist of eight protons and neutrons with the valence space spanning the range $0d_{5/2}$–$0g_{9/2}$. For the nuclei with larger A a core of 20 protons and neutrons was assumed, as discussed in Sec. III. In order to examine the effect of expanding the single-particle bases of the calculations, the calculations were extended to a "large" no-core model space (see Sec. III) for some selected decays. For each degree of forbiddenness one β^- and one EC decay from the mass range $A = 74$–116 were selected, with the exception of the third-forbidden decays were there were only EC decays available. The large no-core model spaces were spanned by 6 or 7 major oscillator shells containing the single-particle states from $0s_{1/2}$ to the $2s$-$1d$-$0g$-$0h$ for $A = 74$–108 and to $2p$-$1f$-$0h$ for $A = 116$. For these selected decays the NME was calculated for three values of g_{ph}: 0.80, 1.00, and 1.20, and for the range $g_{pp} = 0.70$–1.30. The results are presented in Figs. 10–16.

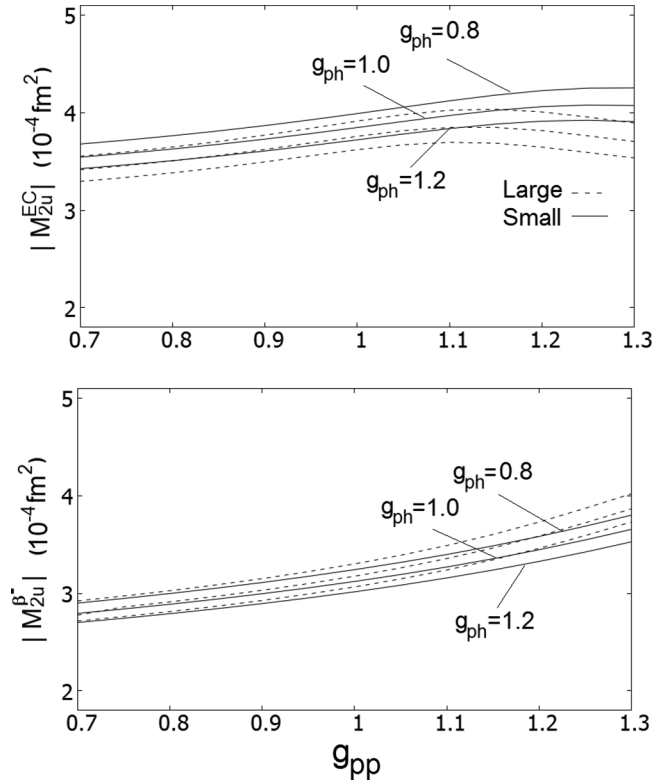

FIG. 10. The NMEs related to the second-forbidden transitions ^{94}Nb$^*(3^+) \xrightarrow{EC} {}^{94}Zr(0^+)$ (top panel) and ^{94}Nb$^*(3^+) \xrightarrow{\beta^-} {}^{94}Mo(0^+)$ (bottom panel) as a function of the scaling parameters g_{pp} and g_{ph}. The solid lines represent the results obtained by using the small model space, i.e., with an inert core, and the dashed lines display the results obtained in the no-core large model space.

For the decays belonging to GROUP 1 there is little difference in the NMEs calculated in the large and small model spaces, with the fourth-forbidden decay ^{104}Rh$(5^+) \xrightarrow{EC}$ ^{104}Ru(0^+) as an exception. As seen in Fig. 12 the nuclear matrix elements calculated using the large and small model spaces differ by about 20–30% for similar values of g_{pp} and

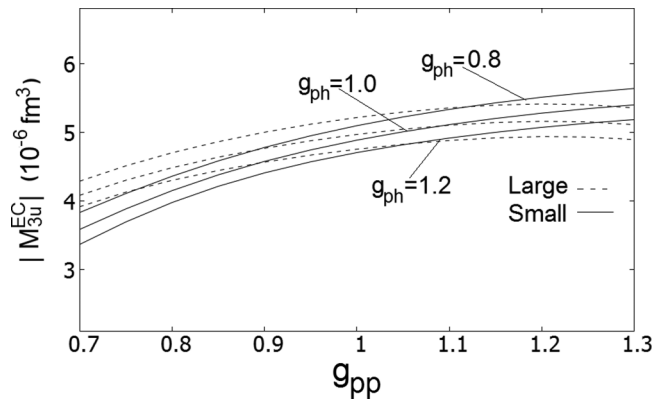

FIG. 11. The same as Fig. 10 but for the third-forbidden transition ^{74}Br$^*(4^-) \xrightarrow{EC/\beta^+} {}^{74}Se(0^+)$.

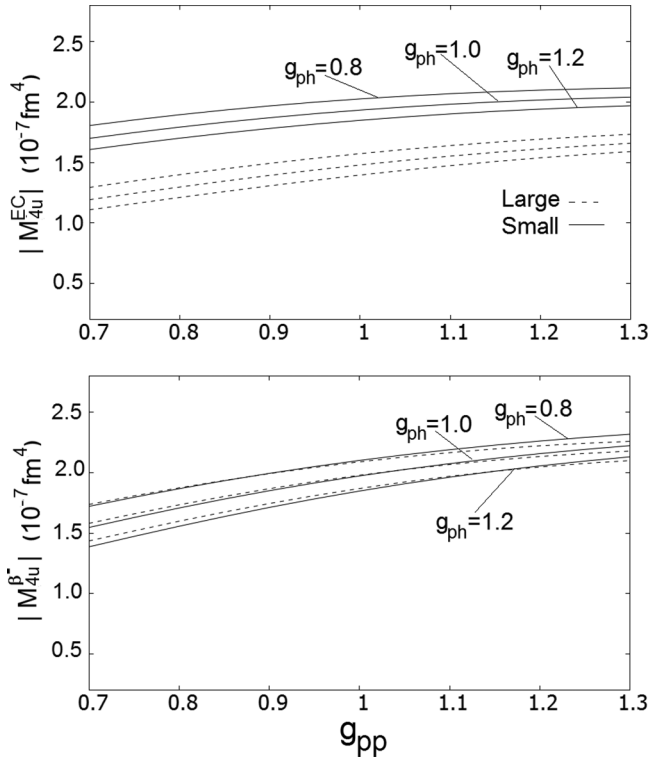

FIG. 12. The same as figure 10 but for the fourth-forbidden transitions ^{104}Rh$^*(5^+) \xrightarrow{EC} {}^{104}Ru(0^+)$ (top panel) and ^{104}Rh$^*(5^+) \xrightarrow{\beta^-} {}^{104}Pd(0^+)$ (bottom panel).

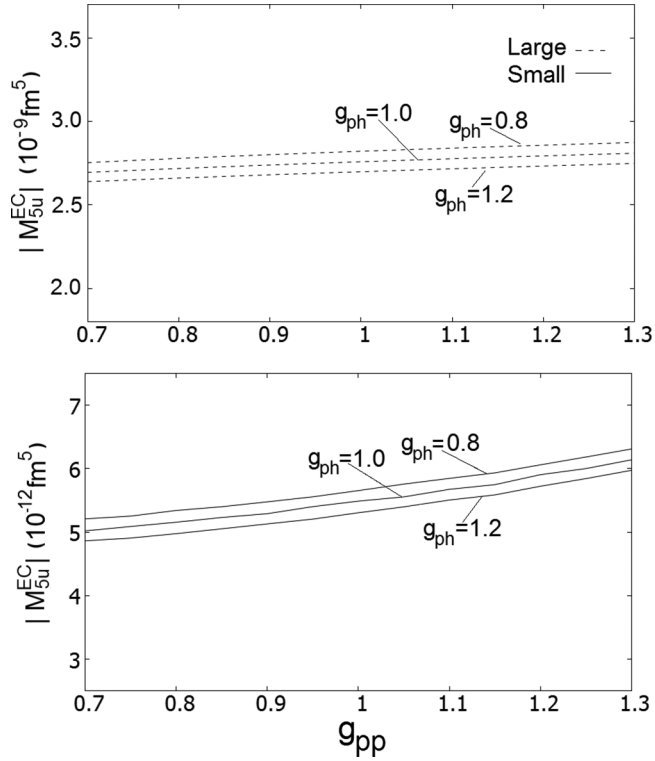

FIG. 13. The same as Fig. 10 but for the fifth-forbidden transition ^{86}Rb$^*(6^-) \xrightarrow{EC} {}^{86}Kr(0^+)$. The results for the large model space are presented in the top panel and for the small model space in the bottom panel.

g_{ph}. The expected half-life for this decay is some 40% longer in the large model space than in the small one.

The differences in the GROUP 2 decays, on the other hand, can be much larger in some extreme cases. For example, for the fifth-forbidden GROUP 2 transition ^{86}Rb$^*(6^-) \xrightarrow{EC} {}^{86}Kr(0^+)$ (see Fig. 13) the difference is three orders of magnitude. As can be seen from Table VIII the decay has an exceptionally small NME in the small basis calculation, and the large-basis calculation restores its value to the same level as is common for the other fifth-forbidden decays. Thus some of the NMEs of GROUP 2 are unstable against variation in the model-space size and the corresponding half-life cannot be computed accurately. This comes back to the earlier-discussed effect of the unstable pairing conditions in the corresponding (semi)magic reference nuclei. Another example, though less striking, is the seventh-forbidden transition ^{116}In$^*(8^-) \xrightarrow{\beta^-} {}^{116}Sn(0^+)$ (see Fig. 16) for which the small model space gives a NME which is approximately 2.3 times larger than that given by the large model space for most values of g_{pp} and g_{ph}. Contrary to the 1^+ Gamow-Teller decays, the computed NMEs depend only very weakly on g_{pp} for the highly forbidden β decays, and the collapse point of the pnQRPA is very far from the g_{pp} values used in the present calculations (see Figs 10–16). The effect of changing the value $g_{ph} = 1.0$ of the particle-hole parameter amounts to only a small shift in the value of the NME, as seen in the figures.

The above investigations suggest that the calculated NMEs are very stable against variations of the g_{pp} and g_{ph} parameters, and that the collapse point of the pnQRPA is far away from the physically acceptable range of these parameters. The NMEs of GROUP 1 can be reliably predicted in the small model space, the maximum deviations from the ones computed in the large no-core model space being less than 30% around the value $g_{pp} = 1.0$, adopted for the half-life calculations. Hence, the computed half-lives of the GROUP 1 decays in Tables IV–IX are accurate enough for experimental verification. On the other hand, the decays of GROUP 2 are not as stable against the variation of the size of the model space as the decays of

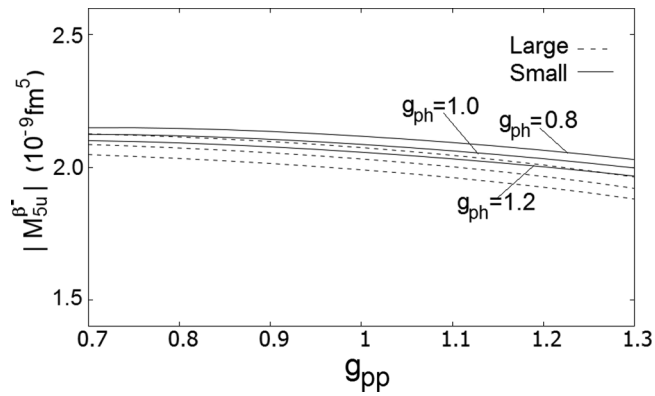

FIG. 14. The same as Fig. 10 but for the fifth-forbidden transition ^{86}Rb$^*(6^-) \xrightarrow{\beta^-} {}^{86}Sr(0^+)$.

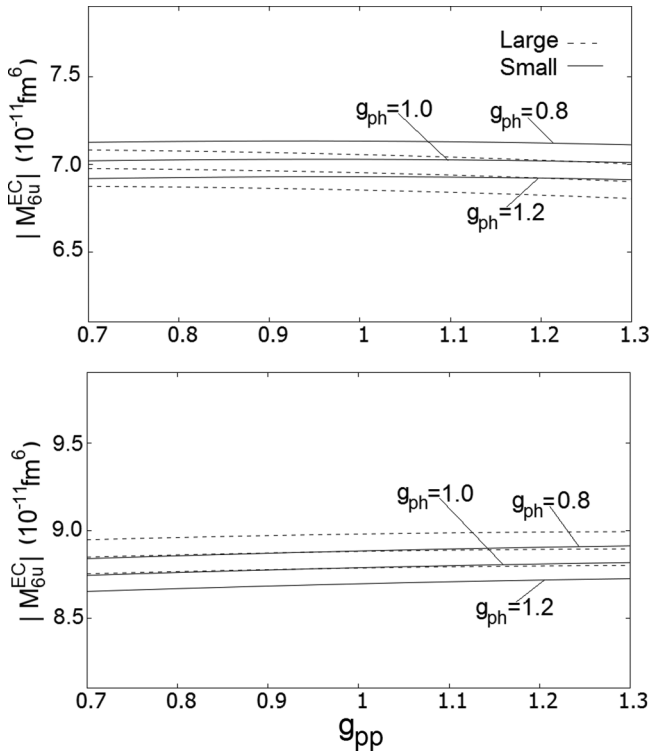

FIG. 15. The same as Fig. 10 but for the sixth-forbidden transitions ^{92}Nb(7^+) $\xrightarrow{EC}$ ^{92}Zr(0^+) (top panel) and ^{92}Nb(7^+) $\xrightarrow{\beta^-}$ ^{92}Mo(0^+) (bottom panel).

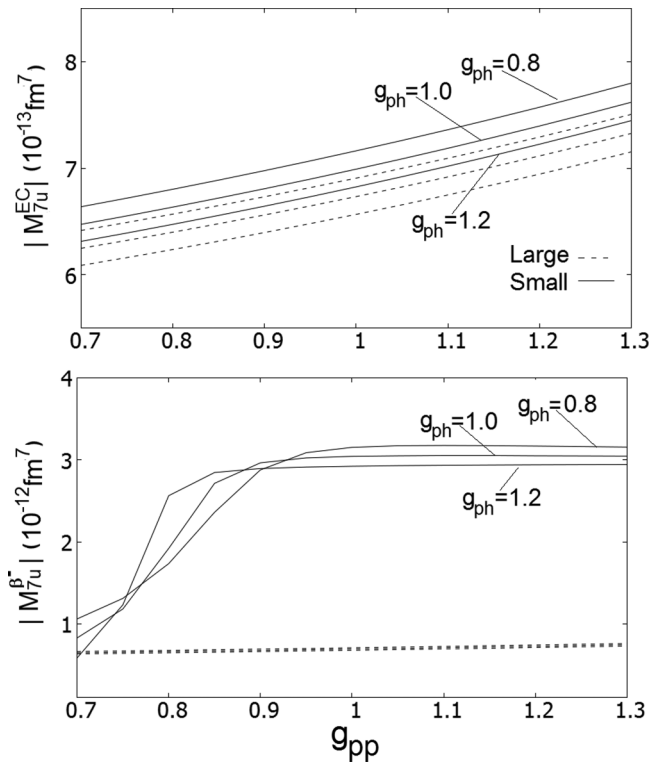

FIG. 16. The same as Fig. 10 but for the seventh-forbidden transitions ^{116}In*(8^-) $\xrightarrow{EC}$ ^{116}Cd(0^+) (top panel) and ^{116}In*(8^-) $\xrightarrow{\beta^-}$ ^{116}Sn(0^+) (bottom panel).

GROUP 1. Since these decays host (semi)magic reference nuclei, small variations in the single-particle energies and in the size of the model space can have a large effect on the NMEs, especially in the cases where the NME is exceptionally small. Thus, for some of these decays the prediction of the corresponding half-life is practically impossible within the theoretical scheme adopted in this work. It should be noted that this does not compromise our main mission of drawing conclusions about the suppression of the high-multipole NMEs relevant for the $0\nu\beta\beta$ decays since the related investigations are performed for the β decays belonging to GROUP 1.

B. Expected half-lives of the decay transitions

The average of the ratios k of the pnQRPA and two-qp NMEs of GROUP 1 agrees relatively well with the value given for allowed GT decays in [11] and the first-forbidden unique SD 2^- decays in [10], as seen in the second and third columns of Table XI. Inspired by the similarity of the GROUP 1 decays to the GT and SD decays, we are led to the plausible conjecture that the ratio $k_{\rm NM} = M_{\rm exp}/M_{\rm pnQRPA}$ for the GROUP 1 decays in the present work is approximately the same as in [11] and [10]. This ratio, as extracted from [11], is approximately a stepwise constant function of the mass number A as shown in the second column of Table XII. The table lists also the factor

$$\xi = (k_{\rm NM})^{-2} = t_{1/2}({\rm exp})/t_{1/2}({\rm pnQRPA}), \qquad (17)$$

which can be used to scale the pnQRPA-calculated half-lives to obtain the expected ones. We make the assumption that the same factors ξ can also be applied to the decays of GROUP 2. Then the factor ξ can be used to calculate the expected "experimental" half-life values, listed in the last column of Tables IV–X. Naturally, it would be of interest to measure (some of) these expected half-lives to see if our conjecture of extrapolating from the allowed GT 1^+ decays and first-forbidden unique SD 2^- decays to the highly forbidden unique decays is accurate enough.

A check of our conjecture would be desirable also for the reason that the factor $k_{\rm NM}$ could be used to scale the pnQRPA NMEs related to the left and right virtual branches of the $0\nu\beta\beta$ decay. The left branch represents the NME related to the virtual transition from the 0^+ ground state of the even-even mother nucleus to a multipole state J^π in the odd-odd intermediate nucleus. The right branch, in turn, connects the same J^π state to the 0^+ ground state of the even-even daughter nucleus. The high-multipole matrix elements computed here represent the low-momentum-exchange limit of the ones involved in the $0^+ \to J^\pi = 3^+,4^-,5^+,6^-,7^+,8^-$ virtual transitions of each $0\nu\beta\beta$-decay branch. In the $0\nu\beta\beta$ decay the virtual transitions go through all the states of the intermediate odd-odd nucleus and the contributions coming from different excitation energies vary strongly from case to case, as discussed in [39]. From the point of view of the exploitation of the present results and the ones of the previous studies on the allowed GT decays [11] and the first-forbidden unique SD 2^- decays [10], a favorable $0\nu\beta\beta$ case would be one in which the dominant contribution(s) come(s) from among the $J^\pi = 1^+,2^-,3^+,4^-,5^+,6^-,7^+,8^-$ multipoles and only few

TABLE XI. Ratio $k = M_{\mathrm{pnQRPA}}/M_{\mathrm{qp}}$ as a function of the mass number A and degree of forbiddenness K for decays belonging to GROUP 1. The results of the earlier works for the Gamow-Teller (GT) and first-forbidden ($K = 1$) decays are quoted for comparison.

A	GT [11]	$K = 1$ [10]	$K = 2$	$K = 3$	$K = 4$	$K = 5$	$K = 6$	$K = 7$	Avg.
50–88	0.35	0.40	0.25	0.46	0.43	0.43			0.39
90–122	0.52	0.40	0.25	0.35	0.34	0.38	0.41	0.13	0.35
122–146	0.40	0.40	0.30	0.28	0.07	0.35		0.19	0.28
Avg.	0.42	0.40	0.27	0.36	0.28	0.39	0.41	0.16	0.34

low-lying intermediate states of the multipole(s) contribute. In the best situation just the lowest-lying state of the involved multipole(s) contributes significantly to the $0\nu\beta\beta$-decay NME, and we can speak about single-states(s) dominance (SSD) of the $0\nu\beta\beta$-decay amplitude (see [39]). In case of SSD the present analysis is the most credible, and scaling by the factor k_{NM} could make sense. However, not even in the simple case of the SSD is it clear how the present low energy and low momentum-exchange study can be extended to the $0\nu\beta\beta$ decay, which is a process of high momentum exchange.

V. CONCLUSIONS

In this work 148 2nd-, 3rd-, 4th-, 5th-, 6th-, and 7th-forbidden unique beta-decay transitions are studied by using the two-quasiparticle (two-qp) and the more sophisticated quasiparticle random-phase approximation (pnQRPA) models. The calculations are done in realistic single-particle model spaces, using Woods-Saxon single-particle energies and a G-matrix based effective two-body interaction. Of special interest is the ratio $k = M_{\mathrm{pnQRPA}}/M_{\mathrm{qp}}$ of the pnQRPA-calculated and the two-qp-calculated nuclear matrix elements (NMEs). The studied decays fall into two categories: GROUP 1, where the even-even reference nucleus is nonmagic, and GROUP 2 where the reference nucleus is (semi)magic, each group sharing half of the studied decay transitions. For GROUP 1 the k value decreases as the mass number increases, while no such behavior is detected for GROUP 2. Except for the seventh-forbidden decays, the degree of forbiddenness does not affect the k values considerably.

Approximately half of the GROUP 2 decays have an exceptionally large k value, around 0.5–0.8. The other half of the decays have a k value less than 0.005, and only a few decays have a k value between 0.005 and 0.5. The differences in k values for GROUP 2 can be three orders of magnitude for the decays of neighboring nuclei. The ambiguous behavior of the decays involving a semimagic nucleus can be traced back to the strong dependence of the corresponding NME on the single-particle energies used in the calculation: A slight change in the energy of a (few) key single-particle orbital(s) can alter the magnitude of the NME by a considerable amount. The dependence of the NME on the single-particle energies is not exclusively a property of the semimagic nuclei, but the dependence is magnified by the use of the BCS approach which gives a sharp Fermi surface and a vanishing pairing gap at magic nucleon numbers. At the same time, and for the above reason, some of the GROUP 2 decays suffer from a rather strong and arbitrary dependence on the size of the adopted single-particle space. In these cases the predicted half-lives are not reliable. The sometimes strong dependence of the NMEs of GROUP 2 on the single-particle energies and the size of the model space leads to the practical conclusion that the predicted half-lives for decays containing (semi)magic nuclei have to be taken with caution since sometimes their errors can be several orders of magnitude.

TABLE XII. Ratio $k_{\mathrm{NM}} = M_{\mathrm{exp}}/M_{\mathrm{pnQRPA}}$ and the factor $\xi = (k_{\mathrm{NM}})^{-2} = t_{1/2}(\mathrm{exp})/t_{1/2}(\mathrm{pnQRPA})$ for different mass regions based on the results in Ref. [11]. Here the geometric mean of the $\beta^{\pm}$ NMEs was used to determine k. The uncertainty of k_{NM} is 10%, which gives ξ an uncertainty of 20%.

A	k_{NM}	ξ
50–96	0.67	2.2
98–136	0.46	4.7
138–146	0.82	1.5

The pnQRPA NMEs of GROUP 1 are reduced by an average factor of $k = 0.29 \pm 0.15$ with respect to the two-qp NMEs, but some dependence on the mass number A and degree of forbiddenness K is recorded. The average suppression of the pnQRPA NME relative to the two-qp NME is in good agreement with the ones found for the Gamow-Teller (GT) 1^+ decays in [11] and the spin-dipole (SD) 2^- decays in [10]. The suppression stems from the spin-isospin correlations which are taken into account at the pnQRPA level but not at the two-qp level, as already noticed in the mentioned earlier studies. Since the transition from two-qp picture to pnQRPA picture affects the highly forbidden unique NMEs roughly the same way as the SD and GT NMEs, the difference between the pnQRPA and the experimental NMEs is most likely also similar. This means that the pnQRPA NMEs can be conjectured to be reduced by an approximate A-dependent factor of $k_{\mathrm{NM}} = 1.5$–4.7 by additional effects, like the nuclear-medium excitations and the many-nucleon correlations going beyond the adopted many-body framework [11]. By this conjecture the factor k_{NM} can be used to derive the expected "experimental" half-lives of the studied decays, listed in the tables of this article. The listed expected half-lives serve as a guide and incentive to adjust the sensitivities of potential experiments trying to measure (some of) these transitions in order to validate or falsify our conjecture.

The suppression factors k and k_{NM}, extracted in the present and previous studies on the subject, could be relevant for the calculation of the values of the NMEs related to the $0^+ \to 1^+,2^-,3^+,4^-,5^+,6^-,7^+,8^-$ virtual transitions involved in the NMEs of the neutrinoless double beta ($0\nu\beta\beta$) decay. In particular, the present results could be of importance in the cases where the virtual transitions are dominated by one or few transitions through low-lying state(s) of the intermediate nucleus [single-state(s) dominance for given multipole(s)].

The present study is the first of its kind and the obtained NMEs can be seen to represent the low-momentum-exchange limit of the ones involved in the $0\nu\beta\beta$ decay. It is not yet clear how the present results can be extrapolated to determine the possible suppression of the NMEs involved in the high-momentum-exchange virtual transitions of the $0\nu\beta\beta$ decay.

ACKNOWLEDGMENT

This work has been partially supported by the Academy of Finland (Suomen Akatemia) under the Finnish Centre of Excellence Programme 2012-2017 (Nuclear and Accelerator Based Programme at JYFL).

[1] H. Behrens and W. Bühring, *Electron Radial Wave Functions and Nuclear Beta Decay* (Clarendon, Oxford, 1982).
[2] M. Haaranen, M. Horoi, and J. Suhonen, Phys. Rev. C **89**, 034315 (2014).
[3] M. T. Mustonen, M. Aunola, and J. Suhonen, Phys. Rev. C **73**, 054301 (2006).
[4] M. Aunola, J. Suhonen, and T. Siiskonen, Europhys. Lett. **46**, 577 (1999).
[5] E. K. Warburton, Phys. Rev. C **31**, 1896 (1985).
[6] J. S. E. Wieslander, J. Suhonen, T. Eronen, M. Hult, V.-V. Elomaa, A. Jokinen, G. Marissens, M. Misiaszek, M. T. Mustonen, S. Rahaman, C. Weber, and J. Äystö, Phys. Rev. Lett. **103**, 122501 (2009).
[7] M. T. Mustonen and J. Suhonen, J. Phys. G **37**, 064008 (2010).
[8] M. T. Mustonen and J. Suhonen, Phys. Lett. B **703**, 370 (2011).
[9] M. Haaranen and J. Suhonen, Eur. Phys J. A **19**, 93 (2013).
[10] H. Ejiri, N. Soukouti, and J. Suhonen, Phys. Lett. B **729**, 27 (2014).
[11] H. Ejiri and J. Suhonen, J. Phys. G: Nucl. Part. Phys. **42**, 055201 (2015).
[12] L. Jokiniemi, J. Suhonen, and H. Ejiri, Adv. High Energy Phys. **2016**, 8417598 (2016).
[13] J. Suhonen, *From Nucleons to Nucleus: Concepts of Microscopic Nuclear Theory* (Springer, Berlin, 2007).
[14] H. Ejiri, Phys. Rep. **338**, 265 (2000).
[15] J. Vergados, H. Ejiri, and F. Šimkovic, Rep. Prog. Phys. **75**, 106301 (2012).
[16] S. R. Elliott and P. Vogel, Annu. Rev. Nucl. Part. Sci. **52**, 115 (2005).
[17] H. Ejiri, J. Phys. Soc. Jpn. **74**, 2101 (2005).
[18] F. Avignone, S. Elliott, and J. Engel, Rev. Mod. Phys. **80**, 481 (2008).
[19] J. Suhonen and O. Civitarese, Phys. Rep. **300**, 123 (1998).
[20] M. Haaranen, P. C. Srivastava, and J. Suhonen, Phys. Rev. C **93**, 034308 (2016).
[21] J. Suhonen and O. Civitarese, Phys. Lett. B **725**, 153 (2013).
[22] J. Suhonen and O. Civitarese, Nucl. Phys. A **924**, 1 (2014).
[23] J. Suhonen and O. Civitarese, J. Phys. G: Nucl Part. Phys. **39**, 085105 (2012).
[24] P. Pirinen and J. Suhonen, Phys. Rev. C **91**, 054309 (2015).
[25] F. F. Deppisch and J. Suhonen, Phys. Rev. C **94**, 055501 (2016).
[26] J. C. Hardy, I. S. Towner, V. Koslowsky, E. Hagberg, and H. Schmeing, Nucl. Phys. A **509**, 429 (1990).
[27] H. Primakoff and S. P. Rosen, Rep. Prog Phys. **22**, 121 (1959).
[28] N. B. Gove and M. Martin, At. Data Nucl. Data Tables **10**, 205 (1971).
[29] E. Ydrefors, M. T. Mustonen, and J. Suhonen, Nucl. Phys. A **842**, 33 (2010).
[30] There is a typo in the corresponding equation (7.188) of [13].
[31] H. Heiskanen, M. T. Mustonen, and J. Suhonen, J. Phys. G: Nucl. Part. Phys. **34**, 837 (2007).
[32] J. Suhonen, Nucl. Phys. A **563**, 205 (1993).
[33] G. Audi and A. H. Wapstra, Nucl. Phys. A **565**, 1 (1993).
[34] G. Audi and A. H. Wapstra, Nucl. Phys. A **595**, 409 (1995).
[35] A. Bohr and B. R. Mottelson, *Nuclear Structure* (Benjamin, New York, 1969), Vol. I.
[36] K. Holinde, Phys. Rep. **68**, 121 (1981).
[37] M. Wang, G. Audi, A. H. Wapstra, H. G. Kondev, M. MacCormick, X. Xu, and B. Pfeiffer, Chin. Phys. C **36**, 1157 (2012).
[38] National Nuclear Data Center, Brookhaven National Laboratory, http://www.nndc.bnl.gov.
[39] J. Hyvärinen and J. Suhonen, Adv. High Energy Phys. **2016**, 4714829 (2016).